CCS Chemistry

MINI REVIEW

Received: June 22, 2025 | Accepted: Aug. 5, 2025 | Published: Oct. 29, 2025

Towards Practical High Energy Density Lithium-Sulfur Batteries

Mengxue He[1†], Yuanrui Li[1†], Mohammadhosein Safari[2] & Quanquan Pang[1*]

[1]*Beijing Key Laboratory for Theory and Technology of Advanced Battery Materials, School of Materials Science and Engineering, Peking University, Beijing 100871,* [2]*Institute for Materials Research (IMO-imomec), UHasselt, Hasselt 3500*

**Corresponding author: qqpang@pku.edu.cn;* [†]M. He and Y. Li contributed equally to this work.

Cite this: *CCS Chem*. **2025**, 7, 3235–3258
DOI: 10.31635/ccschem.025.202506213

Lithium-sulfur (Li-S) batteries have attracted significant attention due to their high theoretical energy density and cost-effectiveness, leading to notable progress in recent years. However, a huge gap between fundamental research and practical implementation remains a major obstacle to commercialization. This review first outlines critical design parameters and technical challenges in realizing practical high energy density Li-S batteries, and summarizes the recent advancements. It then systematically discusses potential strategies to address these challenges, focusing on cathode kinetics, electrolyte optimization, and anode interface engineering. The review further explores the opportunities, challenges, structural designs, and capacity enhancement strategies for next-generation all-solid-state Li-S batteries. Finally, future research directions are proposed to guide the continued development of high energy density Li-S battery technologies.

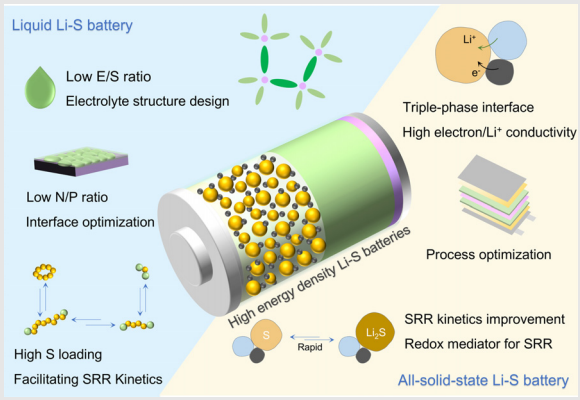

Keywords: **lithium-sulfur batteries, high energy density, cathode kinetics, electrolyte optimization, all-solid-state electrolyte**

Introduction

The rising demand for electric vehicles and portable electronics has accelerated the development of energy storage systems with higher energy density, lower cost, and greater environmental sustainability. Lithium-ion batteries (LIBs), currently the dominant technology, are widely adopted due to their reliable performance. However, their energy density is approaching the theoretical limit (~250–300 W h kg^{-1}), restricting their ability to meet future energy requirements.[1,2] In addition, the limited availability and high cost of critical materials such as cobalt and nickel challenge the sustainability of large-scale deployment. In this context, lithium-sulfur (Li-S) batteries have garnered increasing interest owing to their high theoretical energy density (2600 W h kg^{-1}) and the advantages of sulfur's natural abundance, low cost, and environmental friendliness.[3,4]

The development of Li-S batteries dates back to 1962, when Herbert and Ulam first proposed sulfur as a potential cathode material.[5] However, progress remained limited due to an incomplete understanding of material properties and electrochemical reaction mechanisms. In 2009, Nazar and coworkers[6] introduced mesoporous carbon CMK-3 as a sulfur host, which improved electronic conductivity, suppressed the polysulfide shuttle effect, and alleviated volume expansion, thereby improving sulfur utilization and cycling stability. This work established a foundation for practical Li-S batteries, although challenges such as lithium polysulfides (LiPSs) shuttling and

lithium dendrite growth persisted. In the 2010s, research entered a phase of rapid advancement. To mitigate LiPSs shuttling, various strategies—such as tailored cathode architectures, chemical adsorption, and electrocatalysis—were developed to accelerate reaction kinetics and extend cycling life.[7,8] Concurrently, electrolyte formulations and lithium anode protection strategies were devised to stabilize the electrode–electrolyte interface and further suppress the shuttle effect.[9,10] Since 2014, increasing attention has been directed toward improving the energy density of Li-S batteries. It was revealed that a low electrolyte-to-sulfur (E/S) ratio is critical to increase the energy density. This understanding has led to the development of practical pouch cells by optimizing the E/S ratio, sulfur areal loading, and lithium excess, thus enabling improvements in both energy density and cycling performance.[2,11]

Over the past decade, substantial progress in high-loading electrode fabrication and cathode design has addressed key challenges such as electrode cracking and incomplete sulfur utilization. These innovations have enabled sulfur loadings to increase from 1 to 2 mg cm^{-2} to over 5 mg cm^{-2} without compromising electrochemical performance. Simultaneously, advances in electrolyte engineering have reduced the E/S ratio to below 5 µL mg^{-1}, significantly improving energy density under lean electrolyte conditions.[12] State-of-the-art Li-S pouch cells have demonstrated record energy densities of 695 W h kg^{-1} at the cell level,[13] while typical systems reach 300–400 W h kg^{-1}. However, these pouch cells generally suffer from limited cycle life of less than 100 cycles. Despite energy densities comparable to commercial LIBs, the poor cycling stability—far below the >1000 cycles of LIBs counterparts—remains a major limitation for Li-S batteries.

This review presents a comprehensive overview of recent advances in high energy density Li-S batteries. We first outline the critical design parameters and corresponding technical challenges hindering practical implementation. Strategies to address these challenges are then discussed with a focus on cathode, electrolyte, and anode engineering. The review also highlights advances in all-solid-state Li-S batteries (ASSLSBs), including their structural designs, capacity enhancement strategies, and inherent challenges. Finally, future research directions for developing practical high energy density Li-S batteries are proposed.

Principles and Challenges

Principles of Li-S batteries

A typical Li-S battery consists of a sulfur cathode, a lithium metal anode (LMA), separator, and electrolyte

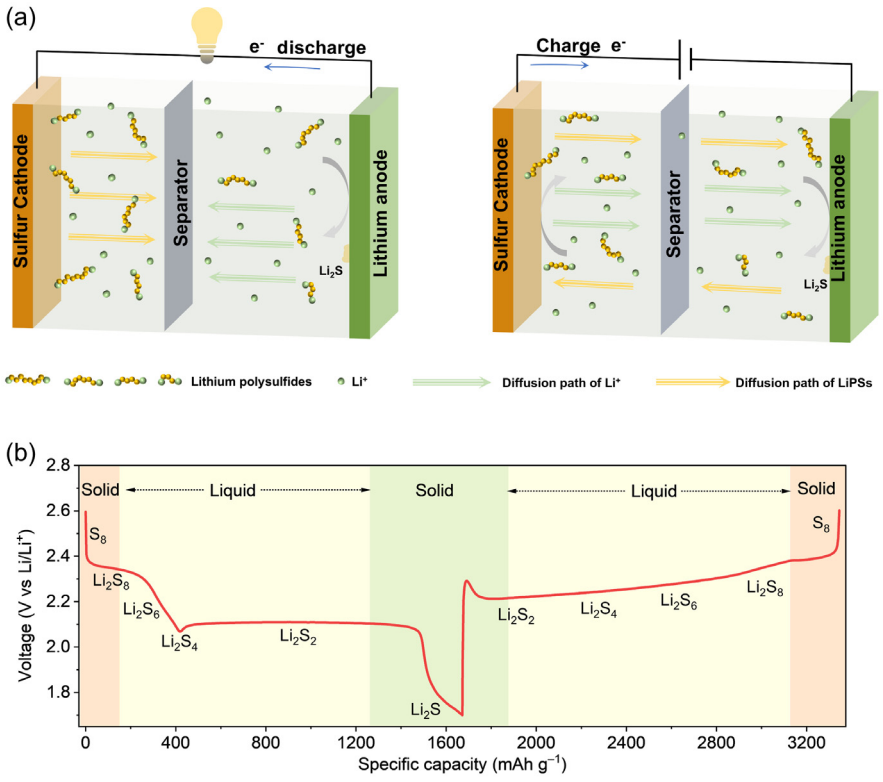

Figure 1 | *Battery configurations and fundamental mechanism of the Li-S battery. (a) Typical Li-S battery configuration and its working principle. (b) Typical discharge and charge voltage profile of the Li-S battery in one cycle.*

DOI: 10.31635/ccschem.025.202506213
Citation: *CCS Chem.* **2025**, 7, 3235–3258
Link to VoR: https://doi.org/10.31635/ccschem.025.202506213

(Figure 1a). During discharge, electrons flow from the LMA to the sulfur cathode via the external circuit, while Li^+ ions are released from the LMA, solvated in the electrolyte, and migrate toward the cathode under an electric field. At the cathode, S_8 molecules accept electrons, undergo ring-opening, and react with Li^+ to form soluble lithium polysulfides (Li_2S_n, $2 \leq n \leq 8$), which are subsequently reduced to insoluble Li_2S (Figure 1a).[3,14] The overall discharge process involves a stepwise 16-electron reduction of S_8. The voltage profile typically features two distinct discharge plateaus: the high-voltage plateau (~2.3 V), where S_8 is reduced to soluble Li_2S_4 via a combination of electrochemical and disproportionation reactions, involving four electrons per S_8 molecule and delivering 418 mA h g^{-1}; and the low-voltage plateau (~2.1 V), where Li_2S_4 is further reduced to solid Li_2S, transferring 12 electrons per S_8 molecule and providing an additional 1254 mA h g^{-1} (Figure 1b).[15,16] Upon charging, this process reverses, with Li_2S gradually oxidized back to solid S_8. This solid–liquid–solid conversion pathway is characteristic of ether-based electrolytes, which remain the most extensively studied system in Li-S battery research.

Parameters and challenges of high energy density Li-S batteries

Gravimetric energy density is a critical parameter for evaluating the practical viability of Li-S batteries. Over the past two decades, significant efforts have been made in electrode structure design, interfacial engineering, and electrolyte formulation, markedly improving the cathode capacity and cycling stability. Coin cells now routinely deliver capacities exceeding 1200 mA h g^{-1} and demonstrate stable cycling over 1000 cycles, even at high current rates. However, these results are often obtained under idealized conditions, including low sulfur loading, excessive electrolyte volume, and excess Li, which diverge from practical application scenarios. To date, few Li-S batteries have demonstrated energy densities greater than 500 W h kg^{-1}. While specific energies surpassing 300 W h kg^{-1} have been reported, their cycle life typically remains below 100 cycles, falling short of practical requirements.[17,18] Table 1 summarizes representative Li-S systems that have achieved high energy densities.

Identifying the key determinants of energy density is crucial for guiding material design, optimizing cell architecture, and bridging the gap between laboratory research and practical applications. We first examine the primary factors affecting the energy density of Li-S batteries to support the development of high energy density Li-S technologies. A typical pouch Li-S battery comprises multiple double-sided sulfur cathodes and lithium anodes, along with a multilayer separator and electrolyte, as illustrated in Figure 2a.[41] It also includes positive and negative current collectors, tabs, and an aluminum-laminated film package. The energy density calculation is based on the following equation:[2,42]

$$\text{Energy density} = 2{,}567\ \text{W h kg}^{-1} \times R_{\text{weight}} \times R_{\text{energy}}$$

where R_{weight} represents the total mass percentage of both S and active Li, and R_{energy} represents the energy utilization ratio, expressed as follows:

$$R_{\text{energy}} = \frac{C_{\text{sulfur}}}{1675\ \text{mA h g}^{-1}} \frac{V_{\text{cathode}}}{2.2\ \text{V}}$$

$$R_{\text{weight}} = \frac{\frac{M_{Li2S}}{M_S} m_{sl}(1 - R_{\text{package}})}{\frac{m_{sl}}{R_{\text{cathode}}} + \frac{m_{Al}+m_{Cu}}{2} + m_{\text{separator}} + \rho_E R_{E/S} m_{sl} + \frac{2M_{Li}}{M_S} R_{N/P} m_{sl}}$$

where C_{sulfur} denotes the specific discharge capacity of sulfur; V_{cathode} is the average discharge voltage of pouch cell; M_{Li2S}, M_{Li}, and M_S represent the molar mass of Li_2S (45.947), Li (6.941), and S (32.065), separately; m_{sl} illustrates the areal sulfur loading in the cathode; R_{package} indicates the mass ratio of package over the total cell mass; R_{cathode} denotes sulfur mass fraction in cathode; and m_{Al}, m_{Cu}, and $m_{\text{separator}}$ represent mass of current collectors and separator. ρ_E is density of electrolyte, estimated with 1.1 mg μL^{-1}; $R_{E/S}$ represents E/S ratio; $R_{N/P}$ represents negative to positive electrode ratio (N/P ratio).

Based on this model, Fei and Li[42] systematically examined the influence of key parameters on energy density. They found that energy density increases exponentially with decreasing E/S ratio decreases, highlighting its critical importance (Figure 2b). Similarly, reducing the N/P ratio significantly enhances energy density by minimizing excess lithium (Figure 2b). Increasing sulfur loading from 1 to 5 mg cm^{-2} markedly improves energy density, although further increases beyond 8 mg cm^{-2} yield diminishing returns (Figure 2c). Under lean electrolyte (E/S <3 μL mg^{-1}) and low N/P (<2) conditions, sulfur content becomes a dominant factor (Figure 2d). Achieving practical energy densities above 300 W h kg^{-1} requires concurrent optimization of key parameters: S loading ≥4 mg cm^{-2}, E/S ≤2.7 μL mg^{-1}, N/P ≤3, and C_{sulfur} ≥1,200 mA h g^{-1}. Under extreme conditions—such as sulfur loading of 15 mg cm^{-2}, 70% sulfur content, reversible capacity of 1200 mA h g^{-1}, an E/S = 1.2 μL mg^{-1}, and N/P = 1.2—the energy density could reach 630 W h kg^{-1}. However, this estimation assumes ideal electrochemical performance, including a discharge capacity of 1200 mA h g^{-1} and an average voltage of 2.2 V. In practice, achieving such performance is challenging, particularly at high sulfur loadings (>5 mg cm^{-2}) and lean electrolyte conditions (E/S <3 μL mg^{-1}), where increased viscosity and sluggish Li_2S precipitation kinetics lead to capacity fade and voltage hysteresis, ultimately reducing the R_{energy}.

DOI: 10.31635/ccschem.025.202506213
Citation: *CCS Chem.* **2025**, 7, 3235–3258
Link to VoR: https://doi.org/10.31635/ccschem.025.202506213

Table 1 | *The Parameters and Electrochemical Performance Comparison of Li-S Batteries*

Cathode	S Loading (mg cm^{-2})	Electrolyte	E/S Ratio (μL mg^{-1})	N/P Ratio	Operating Conditions	Capacity Retention	Energy Density (Wh kg^{-1})	Ref
S/MWCNTs-70%	7.4	0.1 M LiTFSI DME 2.0 wt % $LiNO_3$ 20 mM DMDSe	1.7	~1	25 °C 0.03 C	One cycle	685	13
S-KB-CF_x	6.42 S 2.67 CF_x	0.4 M LiTFSI 0.2 M $LiNO_3$ DME/MTBE	2.5	1.87	25 °C 0.2 mA cm^{-2}	One cycle	661	12
KB/S-70%	8	1.0 M LiTFSI 0.6 M $LiNO_3$ DOL/DME	1.2 1.7	/	25 °C, C/30; 55 °C, C/30	One cycle	481 415	19
TiS_2/S	/	0.4 M LiTFSI 0.2 M $LiNO_3$ DME/MTBE	0.9 1.3	1.1 2	25 °C 0.3 mA cm^{-2}; 0.3 mA cm^{-2}	~40% 17 cycles; 80% 75 cycles;	460 370	20
Li_xMoS_2/S >70%	7.5	1.0 M LiTFSI 0.2 M $LiNO_3$ DOL/DME	2.4	/	25 °C 2 mA cm^{-2}	85.2% 200 cycles	441	17
S-CoFe DASC	12.7	1.0 M LiTFSI DOL/DME 1 wt % $LiNO_3$	2.8	1.29	25 °C ~0.03 C	~68% 10 cycles	436	21
S/MWCNTs-70%	7.5	1.0 M LiFSI 5 wt % $LiNO_3$ DOL/DME 20mM DMDSe	~2.8	~1.2	25 °C 0.2 C	/ 11 cycles	428	22
C/S-70% $Ti_3C_2T_x$ MXene @$CuCO_2O_4$/PE	10.0	1.0 M LiTFSI DOL/DME 1 wt % $LiNO_3$	2.6	2	25 °C 0.2 C	74.2% 100 cycles	417	23
S/CNT/MoS_2	7.1	1.0 M LiFSI 5.0 wt % $LiNO_3$ 0.10 M LiI DOL/DME	~3	~1.3	25 °C 0.05 C	~48.1% 16 cycles	416.4	24
$Co_{5.47}N$@NC/S	5.6	1.0 M LiTFSI DOL/DME 1 wt % $LiNO_3$	2.8	/	25 °C 0.1 C	90% 40 cycles	411	18
KB/S	5	1.0 M LiTFSI 2.0 wt % $LiNO_3$ 1% $LiPO_2F_2$ DOL/DME	2.7	~1	28 °C 80 mA	One cycle	410	25
S/CNT-80% $NiSe_2$ catalyst	17.3	0.6 M LiTFSI 0.4 M $LiNO_3$ DOL/DME	4.0	/	25 °C ~0.05 C	~72.2% 10 cycles	402	26
Co-PCL/S-70%	2.7 3.4	1.0 M LiTFSI 2.0 wt % $LiNO_3$ DOL/DME	3 2.4	1.9 1.5	30 °C 0.05 C	83.6% 20 cycles	330 ~400	27
S/CNT-70%	7.6	1.0 M LiTFSI 2.0 wt % $LiNO_3$ DME/DOL/HME	~3	~1.2	25 °C 0.025 C	56% 27 cycles	387	28
S/CPC@FeS_2-83%	8.4 7.1	1.0 M LiTFSI 0.2 M $LiNO_3$ DOL/DME	3.5 4.0	/	25 °C 0.1 C	98.5% 30 cycles	338 372	29
S/$CoTe_2$/Co-O-NC	6.7	1.0 M LiTFSI 1.0 wt % $LiNO_3$ DOL/DME	4	/	25 °C 0.1 C	~71.4% 25 cycles	368	30

(Continued)

DOI: 10.31635/ccschem.025.202506213
Citation: *CCS Chem.* **2025**, 7, 3235–3258
Link to VoR: https://doi.org/10.31635/ccschem.025.202506213

Table 1 | *(Continued)*

Cathode	S Loading (mg cm^{-2})	Electrolyte	E/S Ratio (μL mg^{-1})	N/P Ratio	Operating Conditions	Capacity Retention	Energy Density (Wh kg^{-1})	Ref
Mo_6S_8/S_8	6.9 S 6.8 Mo_6S_8	0.6 M LiTFSI 0.4 M $LiNO_3$ DOL/DME	1.2	3	25 °C 1 mA cm^{-2}	10 cycles	366	31
CNT/S-80% G-mSnO_2/$SnSe_2$ separator	6.5	1.0 M LiTFSI 2.0 wt % $LiNO_3$ DOL/DME	3	/	25 °C 0.05 C	93.0% 40 cycles	359	32
Super P/S-80% NbN-NbC separator	6.7	1.0 M LiTFSI DOL/DME 1.0 wt % $LiNO_3$	4	/	25 °C 0.05 C	/ 25 cycles	357	33
CNT/S-70%	7.3	0.2 M LiTFSI 5.0 wt % $LiNO_3$ DOL/DME	~3	~1.2 3	25 °C 0.05 C	One cycle	353	34
3d-omsh/ZnS, Co-N-C/S-75%	~6	1.0 M LiTFSI 0.2 M $LiNO_3$ DOL/DME	4 2.5	~2.6	25 °C 0.05 C	~74% 80 cycles	317 ~352.4	7
G@ppy-por/C/S	7	1.0 M LiTFSI 5.0 wt % $LiNO_3$ DOL/DME	3	/	25 °C 0.025 C	91.8% 12 cycles	343	35
CNT/S-80% FVO/CNT@PP separator	5.1	1.0 M LiTFSI 1.0 wt % $LiNO_3$ DOL/DME	3	1.08	25 °C 0.05 C	>95% 12 cycles	341	36
GF/S-75%	4	1 M LiTFSI CPME 50 mM BDTS	3	1.87	40 °C /	~65% 24 cycles	331	37
FeNC-EEB-1/S-70%	8.4	1.0 M LiTFSI 2.0 wt % $LiNO_3$ DOL/DME	3 3	2.1 2.3	25 °C 0.05 C	81% 80 cycles	309.1 320.2	38
IKB/S-80%	4-6	1.0 M LiTFSI 0.3 M $LiNO_3$ DOL/DME	2.5	/	25 °C 0.05 C	~62% 5 cycles	313	39
GF/S-80%	4.6	0.5 M LiTFSI 0.8 M $LiNO_3$ DME/DOL/HMPA	4	1.63	25 °C 0.1 C	86.7% 20 cycles	307	40

MTBE, methyl tert-butyl ether; DASC, diatomic site catalysts; HME, hexyl methyl ether.

To achieve practical high energy density Li-S batteries, it is crucial to reduce the E/S ratio while maintaining high sulfur utilization (>1,200 mA h g^{-1}) at high sulfur content (>70%) and areal loading (>4 mg cm^{-2}). Due to the unique sulfur redox mechanism, the electrolyte volume strongly influences sulfur utilization, necessitating the co-optimization of electrode architecture and electrolyte formulation. Minimizing the N/P ratio is a secondary but still important consideration; however, doing so often compromises cycling stability. In pouch cells, parasitic reactions between LMA and the electrolyte—leading to lithium pulverization and electrolyte depletion—are the primary failure modes. Thus, achieving a Coulombic efficiency (CE) of >99.9% through stable electrolyte systems or robust solid-electrolyte interphase (SEI) engineering is essential for enabling long-cycle-life, high energy density Li-S batteries.

Facilitating Sulfur Reduction Reaction Kinetics for High Loading Electrodes

Achieving high energy density Li-S battery critically depends on maintaining high sulfur utilization under lean electrolyte and high sulfur content conditions. However, thick cathodes with high sulfur loading often suffer from nonuniform reaction kinetics. Under lean electrolyte conditions, the limited solubility of LiPSs impedes their dissolution-diffusion-conversion pathways.[43] Furthermore, the gradual accumulation of insulating Li_2S on the cathode surface blocks electron and ion transport, reducing the effective reaction area. This results in sluggish reaction kinetics, increased polarization, and poor utilization of active materials. Additionally, the dissolution of

DOI: 10.31635/ccschem.025.202506213
Citation: *CCS Chem.* **2025**, 7, 3235–3258
Link to VoR: https://doi.org/10.31635/ccschem.025.202506213

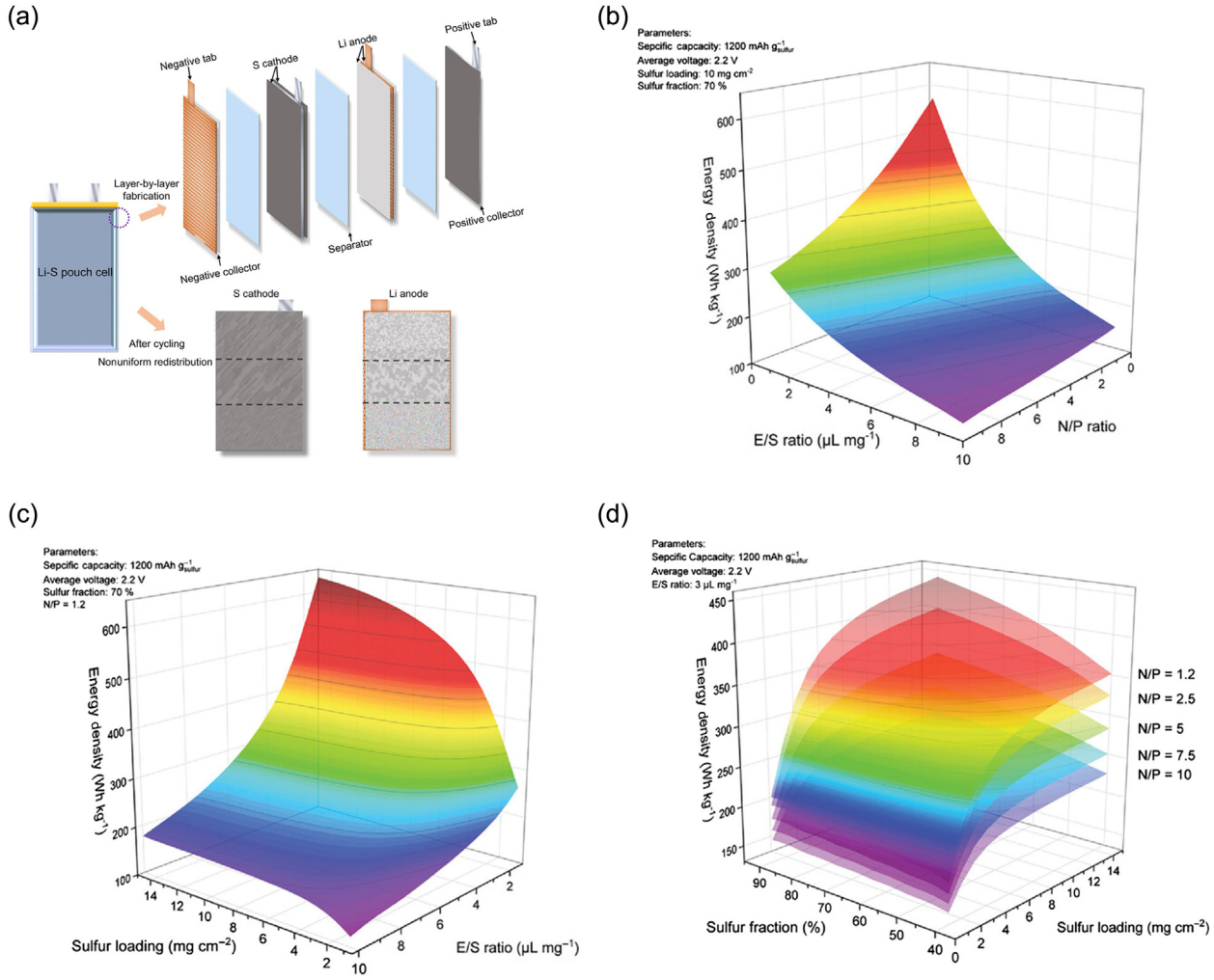

Figure 2 | *(a) Schematic diagram of a multilayer Li-S Pouch cell. Reprinted with permission from ref 41. Copyright 2019 Wiley-VCH. (b–d) Visualization of the cell energy density of Li-S batteries with different sulfur loadings and E/S ratios (b), with different E/S ratios and N/P ratios (c), with different sulfur factions, sulfur loadings, and N/P ratios. Reprinted with permission from ref 42. Copyright 2024 Wiley-VCH.*

abundant LiPSs intermediates aggravates the shuttle effect, leading to active material loss and lithium anode corrosion.

The development of stable and multifunctional cathodes is essential for achieving high capacities in high-loading Li-S batteries. To enhance overall electrode conductivity, various porous carbon materials and conductive polymers have been explored as host frameworks. However, the nonpolar nature of carbon limits its affinity for LiPSs. Polar materials, in contrast, effectively adsorb dissolved LiPSs and provide electrocatalytic sites that accelerate sulfur conversion into short-chain species, enhance sulfur utilization, and mitigate the shuttle effect. Introducing electrocatalysts has thus emerged as a promising strategy to construct high energy density Li-S batteries. These sites typically exhibit strong affinity toward sulfur species. Transition metal compounds—including sulfides,[7,31] carbides,[33] oxides,[32] and nitrides[18]—have shown great promise as electrocatalysts. Additionally, heteroatom-doped carbons,[27] quantum dots, and single-atom catalysts[44] also demonstrate strong electrocatalytic activity toward LiPSs. Integrating catalytic materials—as hosts, additives, or separator coatings—accelerates reaction kinetics and facilitates the development of high-energy-density Li-S batteries. Mo_6S_8, featuring fast Li-ion transport, high electronic conductivity, and intrinsic capacity contribution, serves as an ideal framework for sulfur immobilization. A pouch cell with an intercalation–conversion hybrid cathode achieves 366 W h kg^{-1} and 581 W h L^{-1} under low carbon content and a low E/S ratio.[31] The lithiation of conductive and lyophilic 1T-phase MoS_2 nanosheets can enhance Li^+ adsorption, accelerate electrochemical kinetics, and promote efficient polysulfide conversion, delivering a high energy density of 441 W h kg^{-1} and 735 W h L^{-1}.[17] Ji and coworkers[44] demonstrated that the metal center

DOI: 10.31635/ccschem.025.202506213
Citation: *CCS Chem.* **2025**, 7, 3235–3258
Link to VoR: https://doi.org/10.31635/ccschem.025.202506213

containing exactly two iron atoms maximizes atomic efficiency and regulates sulfur intermediate conversion, achieving 23.8 mA h cm^{-2} at a high sulfur loading of 21.8 mg cm^{-2}. The $Co_{5.47}N$@NC demonstrates remarkable catalytic activity for polysulfide conversion by modulating the d-band center of cobalt atoms, maintaining 1314 mA h g^{-1} at a sulfur loading of 5.7 mg cm^{-2} and E/S ratio of 4.0 μL mg^{-1}. A 1.0 A h pouch cell assembled with this material achieves an energy density of 411 W h kg^{-1}.[18]

The rapid development of catalyst designs has driven deeper investigations into underlying catalytic mechanisms. Electrochemical and in situ characterization techniques facilitate the identification of key discharge products and elucidation of their reaction pathways. In situ Raman spectroscopy and electrochemical measurements reveal that Li_2S_4 is the key intermediate governing sulfur reduction reaction (SRR) kinetics, whereas Li_2S_6 remains electrochemically inactive and exacerbates the shuttle effect.[45] Nitrogen and sulfur dual-doped holey graphene frameworks accelerate LiPSs conversion, enabling rapid depletion of soluble species at elevated potentials, thereby suppressing the shuttle effect and enhancing discharge voltage. In situ UV–vis spectroscopy, synchrotron-based techniques, and theoretical calculations reveal that SRR kinetics are enhanced by increasing LiPSs concentration at the catalyst surface, governed by its antibonding orbital occupancy.[7] This finding enables the modulation of SRR kinetics in various metal catalysts via antibonding orbital engineering. Leveraging this kinetic principle, composite CoZn/carbon catalysts have been developed, delivering stable cycling at high sulfur loading (5 mg cm^{-2}) and high current density (8.0 C). Additionally, Liao and coworkers[46] developed in situ liquid-cell electrochemical transmission electron microscopy (EC-TEM), enabling atomic-scale dynamic, real-time observation of interfacial reactions of the cathode. This technique reveals that Mo NCs/N–G metallic active centers gather soluble LiPSs into droplet-like dense phases, inducing instantaneous crystallization rather than classical step-by-step transformation. Moreover, machine learning has emerged as a powerful tool for catalyst design and optimization. Zhou and coworkers[26] developed a machine-learning-assisted binary descriptor for battery performance, consisting of band match (I_{Band}) and lattice mismatch (I_{Latt}), which together capture the key electronic and structural features of cathode materials. The $NiSe_2$, exhibiting moderate I_{Band} and the lowest I_{Latt}, is predicted—and experimentally confirmed—to accelerate SRR kinetics and improve cycling stability, even at 15.0 mg cm^{-2} and −20 °C. A $NiSe_2$-based pouch cell delivers a specific energy of 402 W h kg^{-1}.

Although numerous materials exhibit promising redox catalytic activity toward sulfur, mechanistic insights into the electrocatalytic process—including reaction pathways and intermediates—remain limited. The lack of standardized metrics for evaluating catalytic activity and efficiency further impedes the development of rational design strategies. To enable the targeted design of Li-S battery electrocatalysts, a deeper mechanistic understanding and the establishment of performance benchmarks are urgently needed. Additionally, many electrocatalysts are electrically insulating and do not contribute to capacity, necessitating conductive additives that compromise both gravimetric and volumetric energy densities. Therefore, enhancing intrinsic catalytic activity and optimizing active sites are central to advancing electrocatalyst performance. Furthermore, economic viability is also critical; ideal electrocatalysts should be low-cost, scalable, and compatible with industrial manufacturing processes.

Electrolyte Design Strategies to Reduce the E/S Ratio

The E/S ratio significantly influences the overall energy density of Li-S batteries. To achieve an energy density over 300 W h kg^{-1} requires reducing the E/S ratio to <3 μL mg^{-1}, with the sulfur electrode's discharge capacity exceeding 1,200 mA h g^{-1}. However, sulfur undergoes a solid–liquid–solid transformation during discharge, where the solubility of intermediate LiPSs governs the reaction kinetics. Consequently, the discharge capacity depends heavily on the electrolyte volume, often showing a direct proportionality. In conventional 1,3-dioxolane/1,2-dimethoxyethane (DOL/DME)-based electrolytes, the maximum LiPSs solubility (~6 mol_S L^{-1}) corresponds to an E/S ratio of ~5.2 μL mg^{-1}. When the E/S ratio falls below 3 μL mg^{-1}, a substantial portion of LiPSs remains undissolved, limiting active material accessibility. Moreover, insulating Li_2S precipitates passivate the electrode surface, impeding further reactions and reducing sulfur utilization—ultimately lowering energy density.

Enhancing the LiPSs solubility theoretically facilitates liquid-phase sulfur conversion, even at low E/S ratios. This has driven the development of high-solvating electrolytes (HSEs). Conversely, suppressing LiPSs solubility enables quasi-solid-state conversion reactions and mitigates dependence on electrolyte volume, motivating interest in sparingly solvating electrolytes (SSEs). These two electrolyte systems exhibit opposing solubility behaviors, leading to distinct discharge mechanisms and corresponding challenges. The following sections discuss the key features and limitations of each system.

Highly solvating electrolyte for Li-S batteries

The dissolution of LiPSs is primarily governed by molecular interactions between electrolyte components and

DOI: 10.31635/ccschem.025.202506213
Citation: *CCS Chem.* **2025**, 7, 3235–3258
Link to VoR: https://doi.org/10.31635/ccschem.025.202506213

LiPSs species. Solvents with high donor numbers (DN) or dielectric constants (ε), such as dimethyl sulfoxide, dimethylformamide, and 1,3-dimethyl-2-imidazolidinone, exhibit strong solvation due to their pronounced Lewis basicity and high polarity.[47,48] Moreover, high-DN solvents also modulate the acid-base environment of coordinated Li^+, facilitating the formation of trisulfur radical anions ($S_3^{\bullet-}$).[49] During discharge, $S_3^{\bullet-}$ acts as an efficient redox mediator, accelerating the conversion of sulfur and long-chain polysulfides to short-chain species, thereby enhancing active material utilization.[50] In addition, the strong Li^+ coordination of high-DN solvents increases the Li_2S solubility and suppresses its deposition kinetics, leading to diffusion-controlled, hemispherical growth via three-dimensional (3D) progressive nucleation.[51] This produces porous, spherical Li_2S particles and delays electrode passivation. During charging, Li_2S dissolution and $S_3^{\bullet-}$ mediation synergistically lower the oxidation overpotential, enhancing redox reversibility.

Although high-DN solvent-based HSEs enhance sulfur utilization under lean electrolyte conditions via improved product solubility and radical-mediated pathways, they still face critical challenges. Their strong reactivity with LMAs leads to unstable Li deposition/stripping and continuous electrolyte degradation, compromising cycling stability. Moreover, the elevated solubility of LiPSs exacerbates the shuttle effect, accelerating capacity decay, lowering CE, and causing severe anode corrosion.

To address these challenges, significant efforts have focused on improving HSEs stability electrolytes via solvent structure modulation, compositional optimization, and tailored structural design, thereby promoting their development and practical implementation. For instance, dual-functional high-DN solvent 3-fluoropyridine is developed to simultaneously enhance LiPSs solubility and LMA compatibility (Figure 3a).[52] This HSE exhibits stable cycling performance even at a high areal sulfur loading of 8 mg cm^{-2}. Additionally, a core-shell structured HSE has been designed through intermolecular interactions between DME/DOL and hexamethylphosphoramide (HMPA), achieving high CE and energy density in Li-S batteries (Figure 3b).[40] Moreover, high-DN co-solvents have also proven effective in improving LiPSs solubility and sulfur utilization.[53,54]

In addition to high-DN solvents, strongly coordinating compounds that interact with Li^+ or S_x^{2-} species can further improve the solubility of LiPSs or Li_2S. For example, high-DN anions (e.g., Br^-, NO_3^-, Tf^-) in DOL/DME electrolytes promote LiPSs dissolution and Li_2S deposition by enhancing Li^+ coordination, thereby improving the discharge capacity.[55–57] Recent study reveals that anions tend to enter the first solvation shell of LiPSs, modulating their solvation structure and formation energy to regulate the reaction kinetics.[58] Furthermore, specific anion receptor is reported to coordinate with S atoms to regulate LiPSs structure and improve Li_2S solubility, promoting 3D Li_2S growth and enhancing discharge capacity under lean electrolyte or low-temperature conditions (Figure 3c).[59] Ji and coworkers[60] demonstrated that cobalt phthalocyanine (CoPc) interacts with sulfur anions in LiPSs, altering their dissociation equilibrium in a DME/DOL electrolyte (Figure 3d). This CoPc-modified electrolyte reduces the cationic LiPSs concentration, effectively suppressing their electromigration toward the LMA during charging. As a result, a high reversible areal capacity of 4.2 mA h cm^{-2} is achieved at a high sulfur loading of 5.0 mg cm^{-2} and a low E/S ratio of 3 μL mg^{-1}. Xi and coworkers[61] demonstrated that 4-mercaptopyridine (4Mpy), serving as a redox regulator, forms lithium-pyridinethiolate, which reversibly participates in LiPSs conversion during charge–discharge cycles, accelerating reaction kinetics and promoting the formation of a 3D Li_2S structure. The Li-S battery with 4Mpy delivers an areal capacity of 10.05 mA h cm^{-2} under a high sulfur loading of 10.88 mg cm^{-2} (Figure 3e).[61]

Extensive research has led to significant progress in HSEs, enhancing electrochemical performance and deepening mechanistic insights into reaction pathways. However, challenges related to cycling stability persist. Addressing these issues requires focused efforts in several key areas. First, molecular-level design of bifunctional solvents that simultaneously stabilize LMAs and promote radical-mediated reactions could significantly improve cycle life. Second, rational cathode architectures are essential to confine soluble LiPSs, suppress the shuttle effect, and promote uniform solid-phase deposition. Third, a deeper understanding of anode interphase evolution and the development of effective passivation strategies—such as high-efficiency additives or artificial SEIs—is crucial for mitigating lithium corrosion and stabilizing electrode–electrolyte interfaces. Finally, advanced in situ techniques, including in situ Raman spectroscopy and X-ray absorption spectroscopy, offer unprecedented insights into LiPSs solvation structures and transformation pathways, providing a theoretical foundation for electrolyte and electrode design. Coordinated efforts across these directions may unlock high-performance Li-S batteries with enhanced energy density and cycling stability, accelerating their practical application in energy storage systems.

Sparingly solvating electrolytes for Li-S batteries

Compared to HSEs, SSEs exhibit extremely low LiPSs solubility (1–10 mM), inducing a transition in the sulfur conversion mechanism from the traditional solid–liquid–solid pathway to a quasi-solid-state process. While trace levels of dissolved LiPSs and localized interfacial reactions may persist, the overall electrochemical conversion becomes largely independent of LiPSs dissolution,

DOI: 10.31635/ccschem.025.202506213
Citation: *CCS Chem.* **2025**, 7, 3235–3258
Link to VoR: https://doi.org/10.31635/ccschem.025.202506213

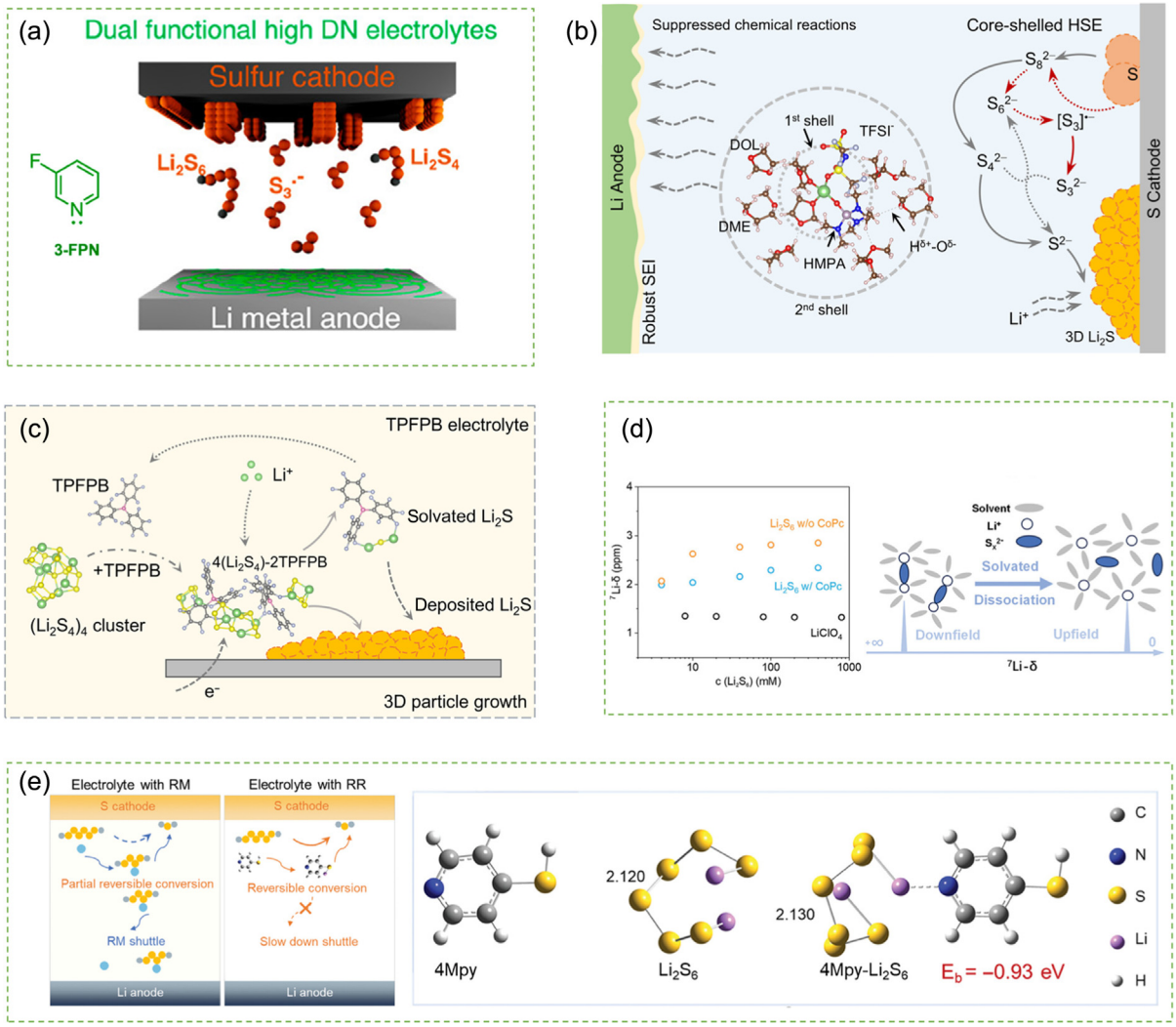

Figure 3 | *(a) Effect of dual functional high donor electrolyte on the sulfur cathode, LMA, and LiPSs redox mechanism. Reprinted with permission from ref 52. Copyright 2022 American Chemical Society. (b) The reaction path of LiPSs and the interface characteristics of LMA in core-shell highly solvating electrolytes. Reprinted with permission from ref 40. Copyright 2025 Wiley-VCH. (c) The schematic mechanism for Li_2S deposition in harsh conditions in tris(pentafluorophenyl)boron electrolytes. Reprinted with permission from ref 59. Copyright 2022 American Chemical Society. (d) The schematic representation depicting the correlation between ^7Li NMR findings and the solvation status of Li_2S_6. Reprinted with permission from ref 60. Copyright 2024 Wiley-VCH. (e) The reaction mechanism of redox mediators and redox regulators in Li-S batteries; the optimized configurations of 4Mpy, Li_2S_6, and 4Mpy-Li_2S_6 specie and their calculated binding energy. Reprinted with permission from ref 61. Copyright 2024 Wiley-VCH.*

rendering the process minimally dependent on electrolyte volume. This makes SSEs particularly attractive for lean-electrolyte Li-S battery systems.

Various electrolyte systems can be classified as SSEs owing to their low LiPSs solubility. Room-temperature ionic liquids (RTILs), composed of organic cations (e.g., imidazolium, pyrrolidinium, piperidinium, and quaternary ammonium) and diverse anions (e.g., $TFSI^-$, $BETI^-$, Tf^-, and BF_4^-), represent a prominent class of electrolytes with limited LiPSs solubility.[62] The solubility of LiPSs in RTILs is governed by the anion Lewis basicity and cation steric hindrance, which collectively affect reaction mechanisms and kinetics. Similarly, solvated ionic liquids (SILs), prepared by equimolar mixing of long-chain glymes (G3 or G4) with lithium salts ([Li(glyme)][X]), show reduced LiPSs solubility due to the formation of stable chelate complexes between glymes and Li^+, which suppress the coordination ability of ether oxygen atoms.[63] Highly concentrated electrolytes (HCEs) also suppress LiPSs solubility by increasing the Li^+/solvent ratio, promoting contact ion pair (CIP) and aggregate (AGG) formation, thereby reducing free solvent availability.[9,64] However, these systems—including RTILs, SILs, and HCEs—often suffer from high viscosity and low ionic

DOI: 10.31635/ccschem.025.202506213
Citation: *CCS Chem.* **2025**, 7, 3235–3258
Link to VoR: https://doi.org/10.31635/ccschem.025.202506213

conductivity. To overcome these limitations, low-polarity solvents are often introduced to form localized highly concentrated electrolytes (LHCEs), which preserve favorable ion–solvent interactions while improving ionic conductivity and discharge performance.[65] Moreover, weakly solvating solvents with low dielectric constants and Lewis basicity have emerged as promising media for SSEs.[66] Their inherently low ability to solvate LiPSs effectively mitigates the shuttle effect while preserving high ionic conductivity. These solvents also promote anion-rich CIP structures even at low salt concentrations, facilitating the formation of anion-derived interphases that stabilize LMAs—crucial for long-life, high energy density Li-S batteries.

Although the SSEs reduce the volume dependence and suppress the shuttle effect via quasi-solid-state conversion pathways, their practical application is hindered by inherently sluggish reaction kinetics, often requiring elevated temperatures and low discharge rate. To address this limitation, our group introduced toluene as a novel diluent which reconstructs the electrolyte microstructure by disrupting aggregates and creating sulfur dissolution microdomains. The toluene-based electrolyte significantly enhances ionic transport, accelerates sulfur redox kinetics, and reduces polarization during operation (Figure 4a).[67] Additionally, other low-density diluents, such as n-hexane and fluorobenzene, have also been explored to optimize the structure of LHCEs for high energy density Li-S batteries.[68,69] Additionally, we explored SSEs incorporating the weakly solvating solvent cyclopentyl methyl ether (CPME). By introducing organic-phase-mediating molecules into CPME-based SSEs, surface-localized polysulfide solvation is promoted, which improves sulfur reaction kinetics and rate capability (Figure 4b).[37] In parallel, Manthiram and coworkers[66] developed a weakly solvating electrolyte using pure tetrahydropyran, enabling stable cycling with high sulfurized polyacrylonitrile (SPAN) loadings (≈5 mg cm^{-2}) and 5 µL mg_{SPAN}^{-1} across a wide temperature range from 0 to 50 °C. Furthermore, cosolvating weakly and moderately solvating solvents has also proven effective in balancing LiPS solubility and improving sulfur kinetics.[70] Although this does not fully establish a quasi-solid-state pathway, it enables high specific capacity at room temperature and mitigates side reactions between LiPSs and LMAs, thus extending the cycle life of high-loading cells (Figure 4c).[71] The low polarity solvents such as hydrofluoroether (HFE),[71] di-isopropyl sulfide,[72] and hexyl methyl ether[73] have also been shown to enhance electrolyte performance. Zhang and coworkers[73] further identified activation polarization, arising from the higher charge-transfer activation energy in rate-determining step, as the primary kinetic limitation. They also observed a two-stage variation with increasing weakly solvating solvent content, determined by whether the solvent penetrates the inner solvation shell of LiPSs. Once the weakly solvating solvent directly coordinates with LiPSs, the charge-transfer kinetics significantly deteriorate, accompanied by a sharp increase in activation polarization. To address this, the incorporation of electrocatalysts has been shown to reduce polarization, prolong cycling stability, and enable high practical energy densities of 607 W h kg^{-1}.[74] Huang and coworkers[75] also demonstrated the activation polarization corresponding to polysulfide oxidation to elemental sulfur is the primary case of discharge capacity loss at high rates. To address the kinetic challenge, the benzo[1,2-b:6,5-b′]dithiophene-4,5-dione was proposed as a redox mediation to accelerate LiPSs oxidation kinetics, thereby improving the rate performance of pouch cells.

The SSEs offer a promising pathway toward high energy density Li-S batteries, but sluggish reaction kinetics remain a major challenge. Future efforts should focus on several critical directions: (1) rational design of cathode architectures to enhance both electronic and ionic transport, thereby facilitating smooth quasi-solid-state sulfur conversion; (2) in-depth mechanistic investigations of sulfur cathode reactions in SSEs using advanced in situ electrochemical, spectroscopic, and computational techniques to guide kinetic optimization; and (3) molecular-level engineering of electrolyte structures to modulate surface-solubilized LiPSs species and address kinetic barriers at ambient temperature.

Low N/P Ratio for Li-S Batteries

A low N/P ratio (<3) is essential for achieving high energy density Li-S batteries, motivating efforts to minimize it in practical cell configurations. However, LMAs undergo continuous capacity fading due to persistent SEI reconstruction and accumulation of inactive "dead" lithium.[76] Ongoing side reactions between LMAs and the electrolyte induce lithium pulverization and electrolyte depletion, both of which are dominant failure modes in Li-S pouch cells. In conventional ether-based electrolytes with a CE of 99%, the capacity retention will drop to 80% after 120 cycles at an N/P ratio of 2 solely due to anode degradation. In addition, parasitic reactions between LMAs and LiPSs produce ionically insulating Li_2S_2/Li_2S species, which elevate interfacial resistance and consume active material, further reducing capacity. These challenges underscore the inferior cycling stability of Li-S cells compared to LIBs, emphasizing that N/P ratio optimization is vital not only for energy density but also for long-term cycle life.

Over the past decade, substantial progress has been made in electrolyte design, SEI engineering, and anode architecture. As the component directly interfacing with LMAs, electrolytes play a critical role in regulating Li deposition/stripping by modulating Li^+ coordination structures. Anion-derived SEI layers, enriched with

DOI: 10.31635/ccschem.025.202506213
Citation: *CCS Chem.* **2025**, 7, 3235–3258
Link to VoR: https://doi.org/10.31635/ccschem.025.202506213

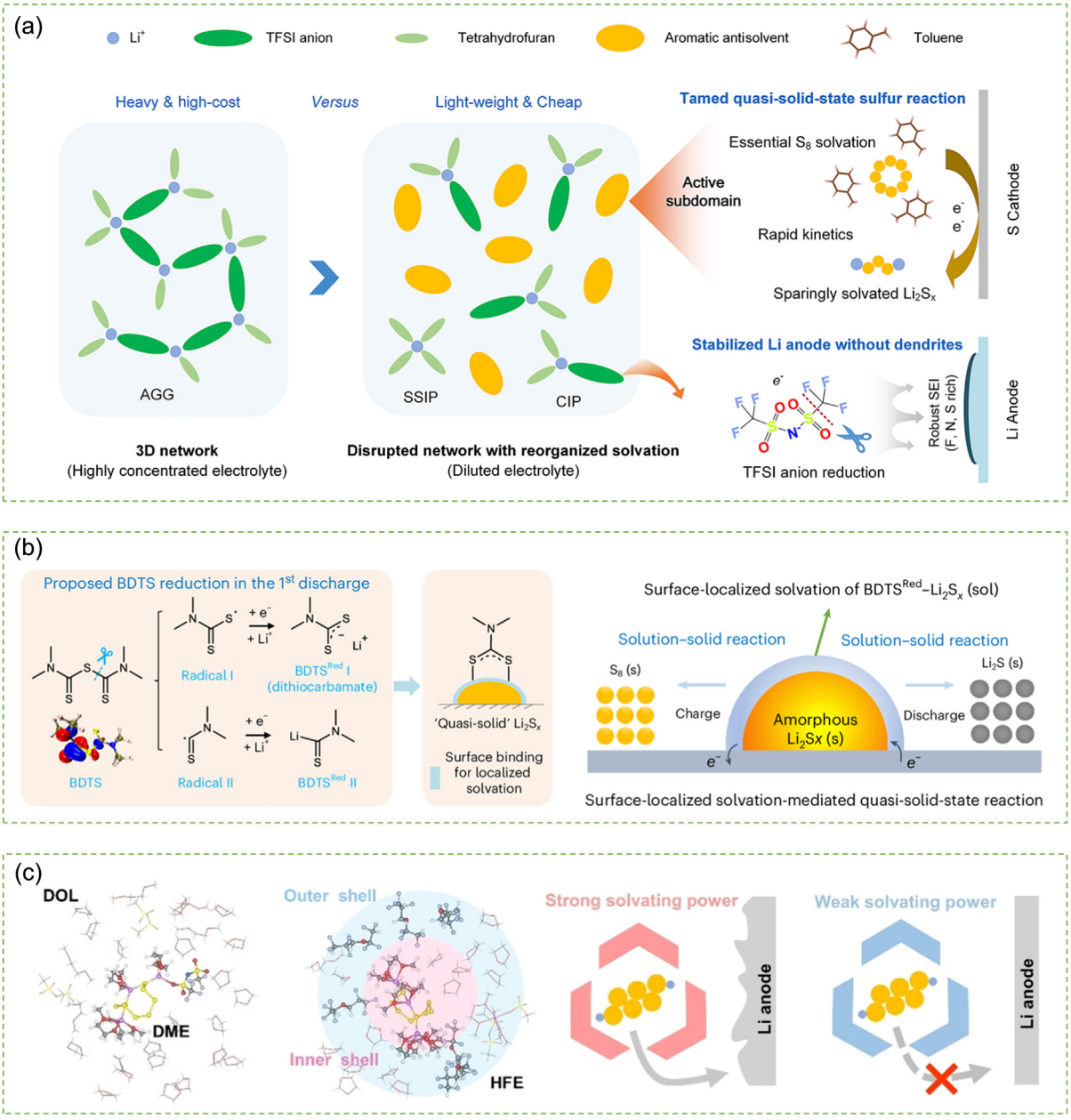

Figure 4 | *(a) The antisolvent-driven restructuring of SSEs for realizing sulfur solvation assisted quasi-solid-state reaction. Reprinted with permission from ref 67. Copyright 2023 Elsevier. (b) The reaction mechanism for bis (dimethylthiocarbamyl) sulfide (BDTS) reduction and its complexing with Li_2S_6; the schematic illustration of the proposed surface-localized solvation-mediated quasi-solid-state sulfur reaction. Reprinted with permission from ref 37. Copyright 2025 Springer Nature. (c) Snapshots of the molecular distributions around S_8^{2-} in the electrolyte with and without HFE, and the scheme of the parasitic reactions between LiPSs and LMA in different electrolyte. Reprinted with permission from ref 71. Copyright 2023 Wiley-VCH.*

inorganic components, have demonstrated improved cycling stability.[37,77] Building on this insight, various electrolyte systems featuring anion–Li^+ coordination—such as HCEs, LHCEs, and weakly solvating electrolytes—have been developed. These systems, characterized by abundant CIPs and AGGs structure, exhibit low LiPSs solubility and are categorized as SSEs. However, their practical application is hindered by sluggish interfacial kinetics. Notably, additives can effectively regulate Li deposition morphology and SEI composition, providing new strategies to overcome these limitations. The potassium 3-thiophenetrifluoroborate (KPTB) facilitates the formation of F-rich SEI and polythiophene-based protective layers on LMA electrodes via preferential redox of PTB^- and K^+-mediated electrostatic shielding, thereby suppressing LiPS corrosion and preserving electrode

DOI: 10.31635/ccschem.025.202506213
Citation: *CCS Chem.* **2025**, 7, 3235–3258
Link to VoR: https://doi.org/10.31635/ccschem.025.202506213

integrity. The electrolyte enables excellent Li-S battery performance across a wide temperature range (−25 to 50 °C) (Figure 5a).[78] The In_2Se_3 functions as a dual-role additive, simultaneously enhancing both cathode and anode performance in lithium-free cells. In_2Se_3 catalyzes LiPSs conversion at the cathode and improves Li deposition reversibility by forming an in situ $LiInS_2$/$LiInSe_2$-containing SEI derived from dissolved In^{3+} and Se^{2-} ions. This additive enables excellent cycling performance in Li-free Li_2S cells (Figure 5b).[79]

The formation and accumulation of "dead" Li significantly deteriorate the battery stability and pose serious safety risks. To address this issue, Huang and coworkers[76] introduced phenethylamine (PEA) to reactivate inactive Li in Li-S batteries. The PEA reacts with inactive Li at the anode to form an organic polysulfide R-LiPEA, which subsequently reacts with the sulfur cathode to generate O-LiPEA. The reversible redox cycle between R-LiPEA and O-LiPEA facilitates lithium reactivation and mitigates capacity fading (Figure 5c).[76] Alloying lithium with metals such as Mg, Al, and Sn offers an effective strategy to stabilize Li anodes by suppressing dendrite formation and buffering volume changes. The anticorrosion Cu-Ni-P (CNP) alloy layer protects the Cu current collector from corrosion and exhibits strong affinity for Li^+, facilitating their Li/Li^+ redox rates and promoting uniform, low-porosity Li deposition (Figure 5d).[80] Li-S batteries with passivated current collectors, a low N/P ratio (1.5), and lean electrolyte (5 μL mg^{-1}) exhibit a tenfold increase in cycle and calendar life. Furthermore, a 3D framework strategy can simultaneously buffer volume fluctuations during Li plating/stripping and suppress dendrite growth by homogenizing current distribution. Zuo and coworkers[81] developed a metal-coordinated 3D porous covalent organic framework (NiS_4-TAPT) incorporating Ni–bis(dithiolene) moieties and nitrogen-rich sites (Figure 5e). The high porosity and uniform channels enhance electrolyte wettability, ensuring homogeneous Li^+ flux distribution and rapid ion transport. Additionally, the abundant N and Ni sites anchor and catalyze polysulfides, suppressing the shuttle effect and improving CE. A full cell using NiS_4-TAPT as both cathode and anode host exhibits high sulfur utilization and stable cycling performance.

Achieving high energy density and long cycle life in Li-S batteries necessitates overcoming challenges associated with LMAs, particularly nonuniform Li deposition/stripping and polysulfide-induced corrosion. To facilitate the practical deployment of Li-S batteries, this work outlines two critical research directions: (1) Elucidating interfacial phenomena at the lithium metal/electrolyte interface, including solvation structures, SEI composition, and Li nucleation/growth dynamics; (2) Evaluating anode protection strategies under practical conditions, including high current densities, high areal capacities, and lean electrolyte volumes suitable for high-loading cathodes.

All-Solid-State Li-S Batteries

Although liquid Li-S batteries have made significant progress in energy density in recent years, ASSLSBs offer a groundbreaking advantage. By using nonflammable solid electrolytes, ASSLSBs not only resolve safety issues but also exhibit remarkable potential for higher energy density. Sun et al.[82] systematically evaluated key parameters—including sulfur content and cathode loading—in pouch cell configurations to compare the energy densities of liquid and ASSLSB. ASSLSBs outperform their liquid counterparts. For instance, at a cathode loading of 6 mg cm^{-2} and 80 wt % sulfur content, ASSLSBs deliver 743 W h kg^{-1}, and the energy density exceeds 1,100 W h kg^{-1} at 18 mg cm^{-2}. These values not only surpass those of liquid Li-S batteries but also exceed the international industry target of 500 W h kg^{-1}.[83–85] This quantitative comparison underscores the superior energy density performance of ASSLSBs.

However, the intrinsic characteristics of solid-state systems pose unique challenges for designing sulfur cathodes. In liquid electrolytes, the electrolyte readily infiltrates electrode pores, enabling continuous ionic transport. In contrast, ASSLSBs require efficient charge transport across complex multiphase interfaces involving active materials (S/Li_2S), conductive carbon, and solid electrolytes.[86] Furthermore, the solid–solid interface between the solid-state electrolyte and composite cathode introduces two primary limitations to charge conduction:[87] first, electronic transport is impeded by the intrinsically insulating nature of sulfur; second, ionic conduction is limited by poor interfacial contact between solid phases. These combined transport limitations render conventional carbon-network-based design strategies less effective in ASSLSBs.

Improvement of electronic and ionic conductivity

In ASSLSB systems, electron transport efficiency critically determines the kinetics of electrochemical reactions. Due to the inherently low electronic conductivity of both S_8 and Li_2S, establishing efficient electron-conductive pathways is essential to sustaining redox processes.[88] To achieve energy densities exceeding 500 W h kg^{-1}, high areal capacities over 5 mA h cm^{-2} are required, which necessitate the use of thick electrodes.[82] However, increased electrode thickness introduces significant challenges. The tortuosity of the triple-phase interfaces (sulfur/conductive additive/solid electrolyte) rises sharply, substantially elevating charge-transfer resistance. Simultaneously, active material utilization drops markedly, often falling below 60%.[86] A more critical issue

DOI: 10.31635/ccschem.025.202506213
Citation: *CCS Chem.* **2025**, 7, 3235–3258
Link to VoR: https://doi.org/10.31635/ccschem.025.202506213

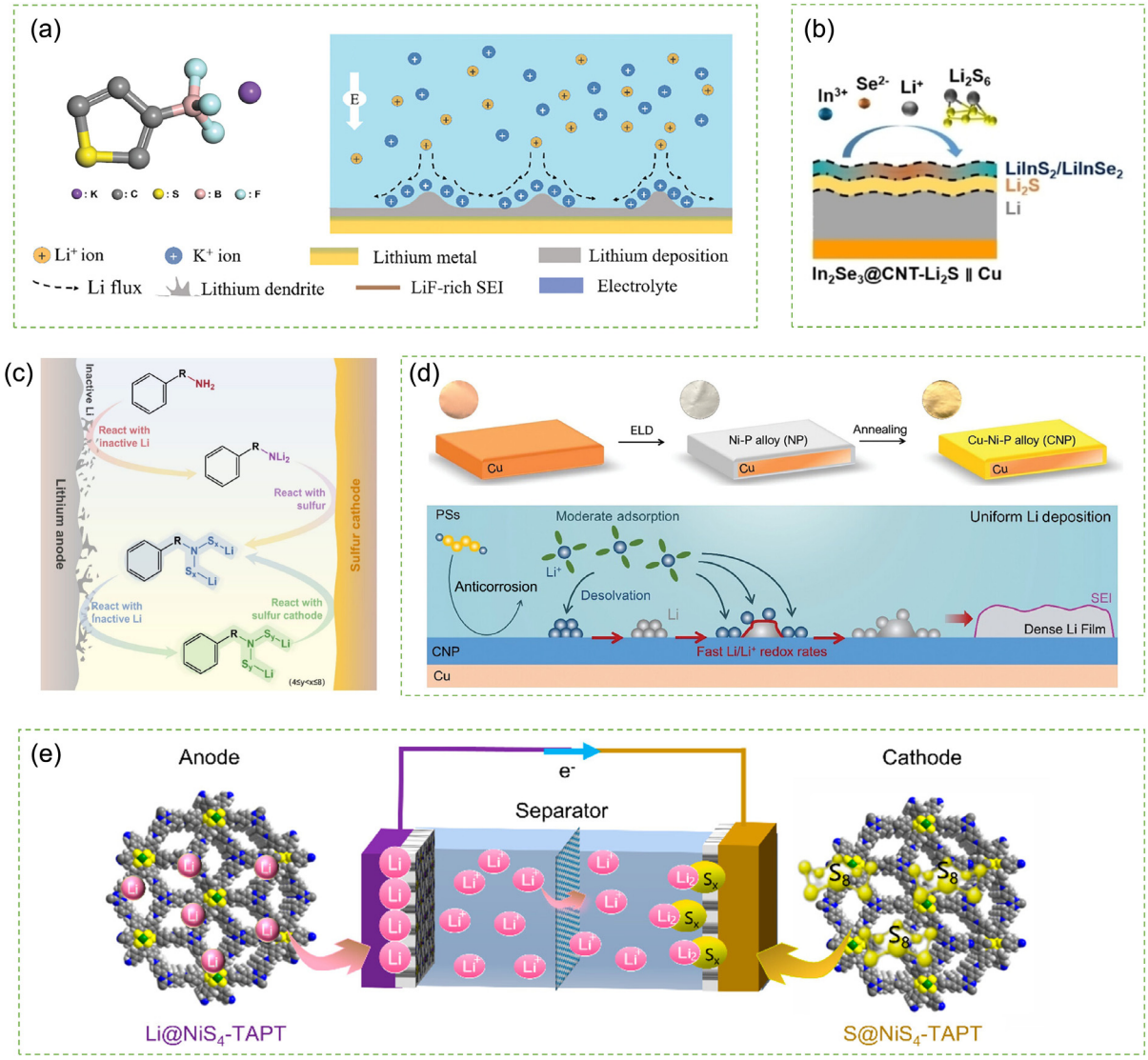

Figure 5 | *(a) Schematic diagram of Li deposition process based on the electrostatic shielding of K^+ in KPTB-incorporated electrolyte. Reprinted with permission from ref 78. Copyright 2025 Wiley-VCH. (b) The effects of In^{3+} and Se^{2-} ions in electrolyte on the formation of the SEI layer on Cu anode and possible reaction Schemes for SEI. Reprinted with permission from ref 79. Copyright 2023 Wiley-VCH. (c) Schematic diagram of the reactivation mechanism of inactive Li through organic polysulfide redox developed from PEA in Li-S batteries. Reprinted with permission from ref 76. Copyright 2025 American Chemical Society. (d) Schematic illustration of the CNP alloy coating preparation and the Li deposition process on the CNP surface with PSs. Reprinted with permission from ref 80. Copyright 2025 Wiley-VCH. (e) Design diagram of a Li-S full battery with NiS_4-TAPT as both the sulfur host material at the cathode side and the lithium host material at the anode side. Reprinted with permission from ref 81. Copyright 2024 American Chemical Society.*

in thick electrodes is that sulfur particles embedded deep within carbon pores fail to maintain effective contact with the solid electrolyte. Moreover, the heterogeneous distribution of the conductive network leads to localized electron transport bottlenecks. Collectively, these factors severely limit the practical capacity output of ASSLSBs.[89] Therefore, a comprehensive understanding and optimization of electron transport mechanisms—particularly through the rational design of conductive networks—are vital for enabling high energy density ASSLSBs.

Researchers have explored various strategies to construct efficient and stable electron transport networks, with carbon materials receiving the most attention due to their excellent electrical conductivity and structural tunability.[90–92] To enable uniform carbon distribution and effective interfacial contact under high sulfur loading, Luo et al.[93] designed a hierarchical carbon nanocage

DOI: 10.31635/ccschem.025.202506213
Citation: *CCS Chem.* **2025**, 7, 3235–3258
Link to VoR: https://doi.org/10.31635/ccschem.025.202506213

(hCNC) that forms a continuous conductive network (Figure 6a). By leveraging multidimensional structural engineering at the particle, interface, and electrode levels, they achieved an ultrahigh areal capacity of 9.95 mA h cm^{-2} under a high sulfur loading of 6 mg cm^{-2}. Beyond carbon architecture, strategies such as halogen/Se doping and nanosizing have also shown to significantly improve sulfur's intrinsic electronic conductivity.[88,94] For instance, Liu et al.[95] demonstrated that iodine doping into the sulfur lattice to form $S_{9.3}I$ molecular crystals significantly increases the conductivity to ~5.9 × 10^{-7} S cm^{-1} at 25 °C—an enhancement of 11 orders of magnitude compared to elemental sulfur. The iodine doping introduces new energy states within sulfur's bandgap, facilitating electron transport and promoting the formation of electrochemically active polysulfides during cycling. Furthermore, the low melting point of $S_{9.3}I$ (~65 °C) enables periodic remelting, which helps heal interfacial damage during operation. As a result, ASSLSB using $S_{9.3}I$ as the cathode material exhibited stable cycling over 400 cycles with 87% capacity retention. This work addresses the long-standing challenge of sulfur's poor conductivity and offers a promising material design strategy for high energy density ASSLSBs.

Although carbon-based conductive networks markedly improve the electronic conductivity of sulfur cathodes, their excessive use in ASSLSBs significantly reduces the active material content, ultimately limiting the achievable energy density. Additionally, sluggish Li^+ transport in solid-state sulfur cathodes severely limits redox kinetics, particularly under high sulfur loading, underscoring the urgent need to optimize ion transport pathways. Various innovative strategies have been proposed to address these challenges.

In interfacial engineering strategies, Whang et al.[96] developed an innovative FeS-Li_2S system that leverages the dual functionality of transition metal sulfides to simultaneously facilitate electron and ion conduction without relying on carbon additives. By optimizing the FeS:Li_2S ratio, the system achieved an areal capacity over 6 mA h cm^{-2} with loading of 10.0 mg cm^{-2}.[96] Zhong et al.[97] employed atomic layer deposition (ALD) to fabricate a lithium phosphorus oxynitride (LPO) interfacial layer on carbon/sulfur particles. The LPO layer serves multiple functions: enhancing Li^+ transport efficiency as an ion-conducting medium, suppressing interfacial side reactions between carbon and electrolyte, and buffering mechanical stress to prevent contact degradation during cycling. This design enabled the full cell to achieve a capacity of 1322 mA h g^{-1} at 0.2C with 86.4% retention over 300 cycles, and an exceptional areal capacity of 11.7 mA h cm^{-2} at 60 °C, highlighting the effectiveness of ALD for interfacial optimization.

The core contradiction in improving electronic and ionic conduction lies in the imbalance between electron transport and ion transport at the interface between solid electrolytes and sulfur cathodes. The operating voltage window of the sulfur cathode is higher than the oxidation potential of the electrolyte, rendering the electrolyte susceptible to oxidative decomposition. Meanwhile, highly conductive carbon materials exacerbate electron transport at the interface, further promoting electrolyte oxidation. Therefore, balancing electron and ion transport at the interface has become a critical challenge. In terms of structural design, Wang et al.[98] designed a hierarchical core-shell ion-conducting architecture via anion exchange at the $Li_{5.5}PS_{4.5}Cl_{1.5}/Li_3YBr_6$ interface (Figure 6b). The $Li_{5.5}PS_{4.5}Cl_{1.5}$ core facilitates fast intraparticle conduction (>5 mS cm^{-1}), while the Li_3YBr_6 shell facilitates interparticle Li^+ transport (>1 mS cm^{-1}). This architecture enables the cathode to retain 85% of its capacity over 1000 cycles at a high areal loading of 8 mg cm^{-2}, and the pouch cell retains 76.9% after 500 cycles. Inspired by the polar group design in liquid-electrolyte Li-S batteries, Nazar and coworkers[99] regulated the charge density and chemical environment at the sulfur host/argyrodite (AG) interface to suppress AG oxidation while preserving ion transport. They adopted a carbon nitride (C_3N_4)-nitrogen-doped graphene (CNG) composite as the sulfur host. The wide bandgap of C_3N_4 limits interfacial electron transport, while pyridinic N sites in CNG strongly interact with Li^+ in AG, effectively tuning the interfacial chemical environment. This configuration inhibits $S^{2-} \rightarrow S^0$ oxidation in AG and prevents subsequent decomposition into insulating by-products. As a result, the battery shows minimal resistance growth over 250 cycles, maintaining an areal capacity of 2 mAh cm^{-2}. Under high sulfur loading, an ultrahigh areal capacity of 11.3 mAh cm^{-2} is attained, offering insights into interface engineering for sulfide-based all-solid-state batteries.

The aforementioned studies underscore the importance of precisely tuning interfacial chemical environments and spatial charge distributions to enhance ion transport efficiency. This insight has spurred new strategies in mixed conductor design that synergistically integrate electronic conduction networks and ion transport channels at the molecular scale—addressing the intrinsic charge transport imbalance in conventional composite electrodes. Cao et al.[100] employed operando neutron imaging and Raman spectroscopy to investigate lithium kinetics in graphite interlayers. Their results revealed the spontaneous formation of Li–graphite interlayers during battery assembly, with Li^+ preferentially depositing at the interface during charging. Continued plating led to the growth of metallic Li dendrites, causing short circuits. Simulations showed that lithium transport is governed by the low nucleation barrier at the interface, shedding light on the complex mechano-chemo-electrochemical coupling in mixed-conductive interlayers. Wang et al.[101] proposed a Li-Ti-P-S mixed ionic-electronic conductor (MIEC) as a replacement for conventional solid electrolytes, effectively reducing the tortuosity of sulfur

DOI: 10.31635/ccschem.025.202506213
Citation: *CCS Chem.* **2025**, 7, 3235–3258
Link to VoR: https://doi.org/10.31635/ccschem.025.202506213

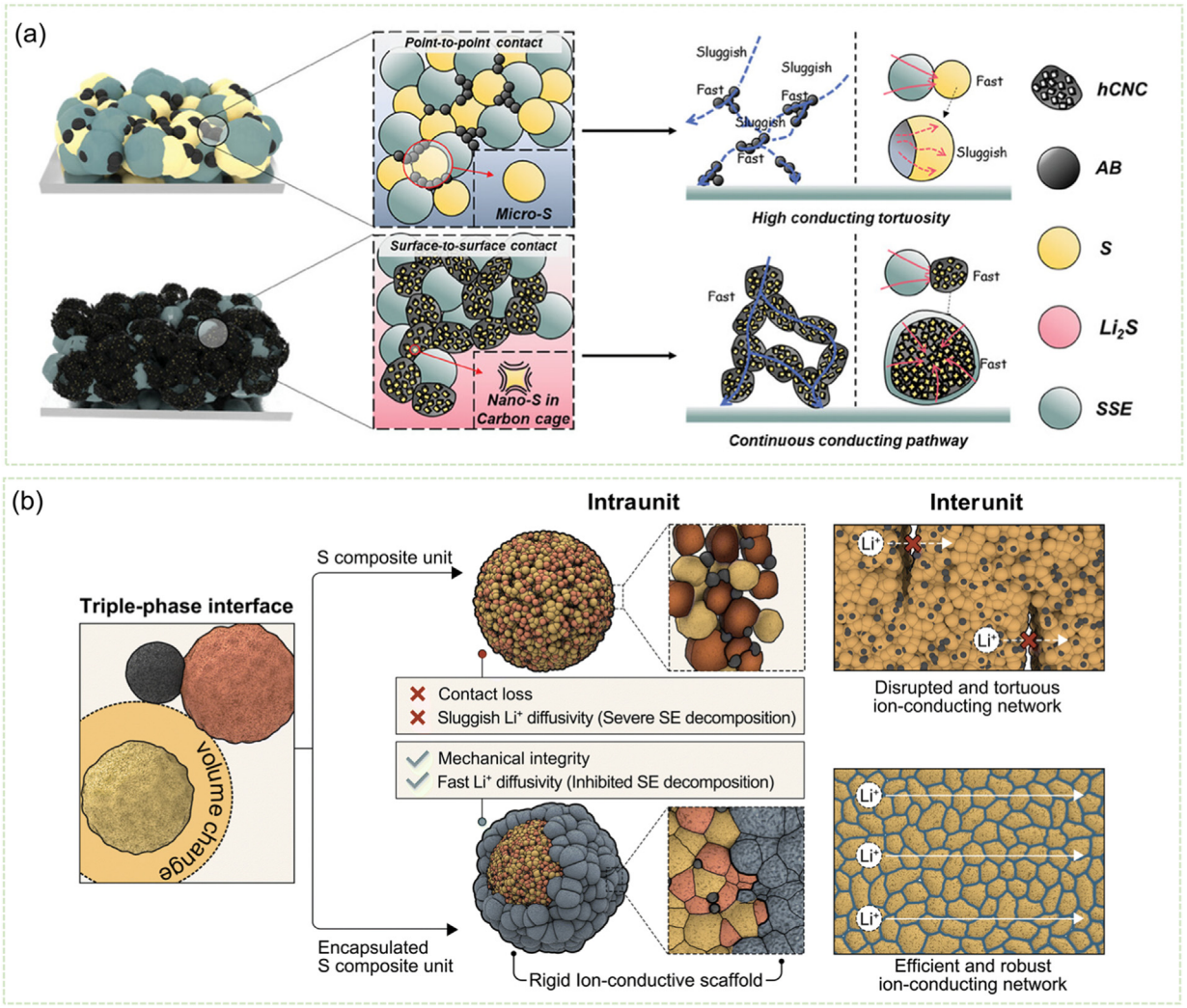

Figure 6 | *(a) Schematic diagram illustrating the advantages of hCNC over AB in enhancing kinetics. Reprinted with permission from ref 93. Copyright 2024 Wiley-VCH. (b) Ion-conduction failure in sulfur cathodes and unitized encapsulation design. Reprinted with permission from ref 98. Copyright 2025 Royal Society of Chemistry.*

composite electrodes. This design establishes a continuous dual-conduction network (electronic conductivity: 10^{-3} S cm^{-1}, ionic conductivity: 1.2 mS cm^{-1}), enabling a high active sulfur content of 87.3%. Experiments confirmed the formation of a uniform, Ti-rich interfacial layer on sulfur particles, with synchrotron analysis revealing structural reversibility during cycling. Compared to traditional triple-phase boundary designs, this strategy increased sulfur loading to 50 wt %, enabling stable cycling for 1000 cycles at 6.8 mA cm^{-1} with a conversion rate exceeding 94%. Moreover, this MIEC strategy was extended to other high-energy conversion-type cathodes, consistently achieving enhanced active material utilization and rate performance—demonstrating its universality and multifunctionality.

In contrast to conventional composite cathodes that require conductive additives to enhance mixed conduction, Cui et al.[102] developed an intrinsically mixed-conductive, zero-strain cathode material, $Li_{1.75}Ti_2(Ge_{0.25}P_{0.75}S_{3.8}Se_{0.2})_3$, synthesized via cold pressing. This material exhibits outstanding dual-conductivity—ionic conductivity of 0.22–0.66 mS cm^{-1} and electronic conductivity of 242–412 mS cm^{-1}—during cycling, while undergoing minimal volume change. The homogeneous cathode, composed entirely of this material, enables ASSLSBs to achieve remarkable cycling stability, retaining 70% of their capacity after 20,000 cycles at 2.5C, and delivering a high energy density of 390 W h kg^{-1} at 0.1C. These advances not only clarify the underlying mechano-chemo-electrochemical coupling mechanisms in mixed conductors but also provide a theoretical framework for designing next-generation, high-efficiency ion transport networks.

The rational design of efficient electron/ion transport networks is the crucial key for enhancing electronic and ionic conductivity. Future research should focus on

DOI: 10.31635/ccschem.025.202506213
Citation: *CCS Chem.* **2025**, 7, 3235–3258
Link to VoR: https://doi.org/10.31635/ccschem.025.202506213

precisely tuning parameters such as pore size distribution and morphology of porous carbons via advanced fabrication strategies. Concurrently, sulfur loading methods must be optimized to ensure intimate contact with the conductive matrix while preserving sufficient pathways for electrolyte infiltration. These advances will stabilize transport channels and hold significant potential for improving the performance of ASSLSBs.

Kinetics enhancement of the sulfur cathode

In optimizing reaction kinetics for ASSLSBs, the synergistic design of interface engineering and catalysis has shown significant promise. Liu et al.[103] modulated the p-band center of the tetrahedron in Li_6PS_5Cl through Sb/O codoping, enabling the in situ formation of a stable $Li_xSb_yS_z$ protective layer at the anode interface. This protective layer stabilized the lithium symmetric cell for over 4000 h while concurrently suppressing sulfur side reactions at the cathode. Simultaneously, this approach suppressed sulfur side reactions at the cathode interface. The fabricated ASSLSB exhibited a specific capacity of 932.6 mA h g^{-1} at 0.1C and maintained 83.7% capacity over 150 cycles, with the pouch cell also demonstrating excellent cycling performance and safety. Cao et al.[104] encapsulated small-molecule sulfur and catalyst clusters within sub-2 nm micropores, constructing molecular-level sulfur-catalyst-carbon interfaces. This strategy resolved the longstanding challenge of achieving molecular contact in solid-state catalysis and buffered sulfur volume fluctuations via a micropore volume of 2.0 cm^3 g^{-1}. The assembled battery exhibited a specific capacity exceeding 1000 mA h g^{-1} at 1.0 C, with a capacity retention rate of over 85% after 1400 cycles. Expanding on the understanding of discharge mechanisms, Sun et al. revealed that the discharge products comprise both Li_2S and Li_2S_2,[105] challenging the conventional assumption of Li_2S dominance. By tuning the discharge cutoff potential and incorporating trace LiI as a solid-state catalyst, Li_2S_2-rich products were favored. This approach enabled the cell to achieve a reversible capacity of 979.6 mA h g^{-1} at 25 °C under 2.0 A g^{-1} and maintain stable cycling for 1500 cycles. Their work not only redefines ASSLSB discharge chemistry but also offers a viable pathway for performance enhancement.

Redox mediation, a proven strategy for accelerating reaction kinetics in liquid Li-S batteries, also offers distinct advantages in ASSLSBs. Yu et al.[106] designed an innovative Li_2S-$Li_xIn_2S_3$ composite cathode, where In_2S_3 serves as a redox mediator, forming a bifunctional material via high-energy ball milling with Li_2S. This architecture mitigates ion/electron transport limitations and volume expansion, delivering an initial areal capacity of 3.47 mA h cm^{-2} (78% Li_2S utilization) at a 4.0 mg cm^{-2} sulfur loading, with 82.35% capacity retention over 200 cycles. Notably, a high areal capacity of 4.08 mA h cm^{-2} is maintained even at a sulfur loading of 6.6 mg cm^{-2}. To address interfacial instability in sulfide electrolytes, Shen et al.[107] developed a novel $Li_{6+x}P_{1-x}W_xS_5I$ (LPWSI) electrolyte that enhances interfacial redox reversibility. The WS_2-derived mixed conductive network facilitates the reversible conversion of $Li_4P_2S_7$ to Li_3PS_4, preventing irreversible $P_2S_7^{4-}$ accumulation (Figure 7a). ASSLSBs employing the LPWSI electrolyte deliver an initial areal capacity of 1.95 mA h cm^{-2} at 0.2C, with 92.2% capacity retention over 400 cycles, and stable cycling for 1000 cycles at high rates (1C/2C). This work offers insights into electrolyte engineering for high-capacity conversion-type electrodes. Most notably, Pang's team[108] developed a lithium thioborophosphate iodide (LBPSI) glass electrolyte, where the $I^-/I_2/I_3^-$ redox shuttle significantly promotes efficient sulfur-to-Li_2S conversion, enabling a fast-charging capacity of 432 mA h g^{-1} at 150 C and 60 °C (Figure 7b,c). More impressively, the assembled battery demonstrates extraordinary cycling stability, retaining 80.2% capacity after >25,000 cycles at room temperature. This breakthrough performance stems from LBPSI's multifunctional nature: during fast charging, surface-generated I_2 and I_3^- transform the constrained three-phase interfacial reaction into a more favorable two-phase reaction, dramatically improving solid–solid sulfur redox kinetics. This achievement not only reinvigorates confidence in Li-S batteries but also opens new avenues for high energy-density ASSLSBs.

In summary, there are still three issues regarding the kinetics of ASSLSBs at present. First, the interfacial reaction kinetics remain to be optimized. Second, the conversion mechanism of discharge products is unclear, and the misjudgment of conversion pathways makes it difficult to precisely regulate the reaction kinetics. Third, sluggish kinetics under high sulfur loading lead to substantial performance degradation. From the perspective of material design, future research needs to break through the density limitation of traditional redox mediators, and develop low-molecular-weight, high-activity lightweight materials. These materials should be able to accelerate the electron transfer between S and Li_2S through reversible redox reactions, while forming stable nanoscale contacts with sulfur and electrolytes, thereby alleviating performance degradation under high loading.

Process optimization

Optimizing the performance of ASSLSBs demands a holistic design strategy that integrates multiscale structural engineering with kinetic regulation. At the microscopic level, tailoring the interfacial chemistry between active materials and electrolytes enhances mass transport. At the mesoscale, optimizing pore architecture and conductive network distribution reduces ionic and electronic transport resistance. At the macroscopic level, electrode architecture and processing strategies

DOI: 10.31635/ccschem.025.202506213
Citation: *CCS Chem.* **2025**, 7, 3235–3258
Link to VoR: https://doi.org/10.31635/ccschem.025.202506213

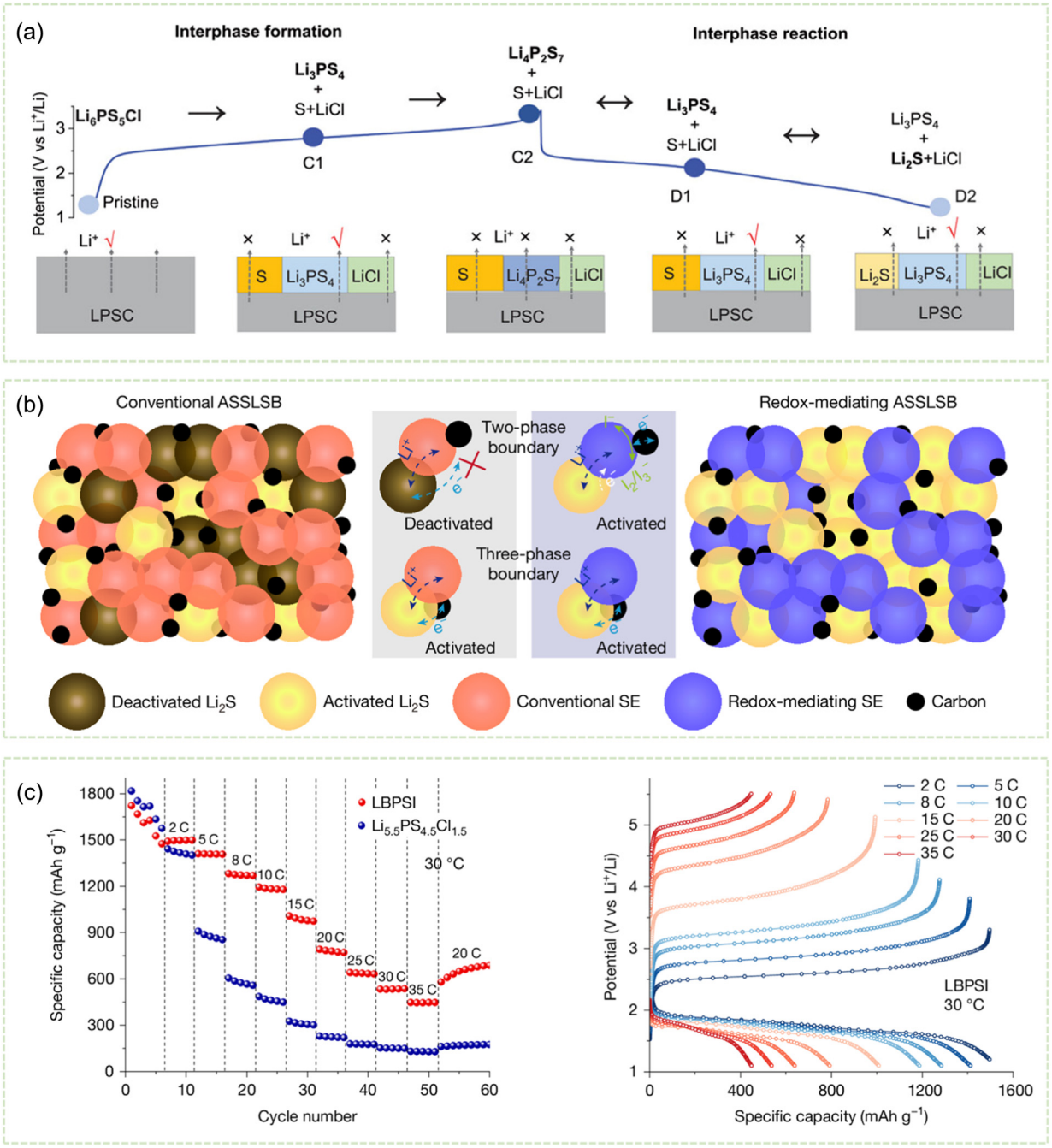

Figure 7 | *(a) Interfacial evolution mechanism of LPSC electrolyte during charge/discharge processes. Reprinted with permission from ref 107. Copyright 2025 Wiley-VCH. (b) Fundamental concept and characterization of the LBPSI glass-phase solid electrolytes. (c) Fast-charging performance of ASSLSBs. Reprinted with permission from ref 108. Copyright 2025 Springer Nature.*

critically influence mechanical integrity and cycling stability. This multiscale, integrated approach offers a promising paradigm for overcoming intrinsic performance limitations in ASSLSBs.

In the development of ASSLSBs, researchers have tackled key challenges through multidimensional innovations. Wang et al.[109] reported a liquid-phase synthesis method to produce a low-density (1.491 g cm^{-3}), small-sized (~500 nm) Li_3PS_4-2$LiBH_4$ glass-ceramic electrolyte, significantly improving the electrolyte volume ratio in cathodes. This strategy enabled cathodes with 60 wt % sulfur loading to achieve 1,144.6 mA h g^{-1} capacity at 60 °C by establishing efficient ion transport pathways in high-loading electrodes. Future research should focus

DOI: 10.31635/ccschem.025.202506213
Citation: *CCS Chem.* **2025**, 7, 3235–3258
Link to VoR: https://doi.org/10.31635/ccschem.025.202506213

on developing new sulfide/halide electrolyte systems with inherently low lattice density, while simultaneously optimizing particle morphology and packing configurations to control electrolyte density without compromising ionic conductivity.[110] Such intrinsic material-based lightweight strategies offer distinct advantages over composite modification approaches, particularly in simultaneously achieving high ionic conductivity and interfacial stability. This approach provides a more robust and fundamental route toward high energy density ASSLSBs by addressing inherent material properties rather than relying on secondary modifications.

While optimizing electrolytes is essential, advancing electrode fabrication techniques is equally crucial for improving the performance of ASSLSB. Current strategies involving the mixing of sulfide-based solid electrolytes with sulfur solutions[111,112] or the addition of minimal liquid-phase solutions[113,114] can achieve interfacial integration but often require expensive and complex processing steps. In contrast, Kim et al.[115] proposed a two-step ball milling method that integrates high-energy milling with gentle mixing. This dry processing method not only avoids complex liquid treatments but also facilitates the in situ formation of lithium-ion conductors via chain reactions between sulfur and Li_6PS_5Cl (LPSCl). The method preserves the high ionic conductivity of LPSCl and markedly enhances three-phase interfacial contact within the sulfur cathode. Using this method, the cathodes delivered an areal capacity of 10.1 mA h cm^{-2} at 30 °C and retained 92.0% capacity retention after 150 cycles. This strategy offers a simpler and more scalable route for fabricating high-loading sulfur cathodes.

The development of practical ASSLSBs faces significant challenges in electrode fabrication technology. While lab-scale powder pressing enables high-quality electrodes, it is unsuitable for large-scale production due to its complexity and inefficiency. This limitation is particularly pronounced for pouch cells and high-loading electrodes, which require scalable, continuous electrode sheet manufacturing.[116] Although conventional slurry-casting methods can produce sheet electrodes, they suffer from undesirable reactions between solvents and sulfide electrolytes. To address this, solvent-free dry processing has emerged as a promising alternative. Notably, Hippauf et al.[117] developed a 150 μm-thick electrolyte membrane using a polytetrafluoroethylene (PTFE) binder, achieving a conductivity of 2.7 mS cm^{-1}. Hu et al.[118] successfully assembled pouch cells delivering a discharge capacity of 9.2 mA h at a sulfur loading of 2 mg cm^{-2}. Fiedler et al.[119] fabricated self-supporting cathodes with just 0.1 wt % PTFE, achieving 1661 mA h g^{-1} at 0.1 C and 72% capacity retention after 400 cycles. Yang and coworkers[120] developed high-performance ASSLSBs using a dry-processing technique to fabricate sulfur-composite cathodes and solid electrolyte membranes. The cathodes achieved an areal loading of 4.5 mg cm^{-2} with sulfur content of 40 wt %, remaining 76% capacity retention over 100 cycles at 0.5 mA cm^{-2} and 0.1C, comparable to conventional powder-based electrodes. The dry-processed electrolyte membrane exhibited a high ionic conductivity of 1.26×10^{-3} S cm^{-1}. Full cells with prelithiated silicon anodes retained 1067.4 mA h g^{-1} after 30 cycles at 1 mA cm^{-2} (0.2C).

These studies reveal that advances in dry processing not only bridge the gap between laboratory research and industrial scale-up but also lay the groundwork for the commercialization of high energy density ASSLSBs. By eliminating solvent-related side reactions, enabling continuous manufacturing, preserving electrochemical performance, and offering scalability, this method emerges as a promising platform technology for next-generation solid-state batteries. Despite these breakthroughs, significant challenges remain for large-scale manufacturing. Future research should prioritize the development and optimization of dry fabrication technologies tailored for industrial needs. In particular, designing highly compatible composite binders is crucial to enhancing interfacial adhesion among electrode components while ensuring compatibility with electrolytes, active materials, and other cell constituents. These improvements are essential for boosting the mechanical integrity and cycling stability of ASSLSBs.

Conclusions and Outlook

This review systematically examines the fundamental mechanisms and key technical challenges of high energy density Li-S batteries. Under practical conditions, achieving theoretical energy densities remains hindered by the limited capacities of high sulfur loading cathodes operating with lean electrolytes. The N/P ratio serves as a dual-functional parameter, simultaneously affecting both energy density and cycle life. We summarize recent advances in cathode kinetics, electrolyte formulation, and lithium metal interface engineering, highlighting effective modification strategies. Given the potential of ASSLSBs for improved safety and energy density, strategies to enhance areal discharge capacity are discussed, focusing on electrode architecture, solid electrolyte design, interfacial modulation, and scalable fabrication.

Despite progress, practical Li-S systems still face major barriers to concurrently achieving high energy density (>400 W h kg^{-1} at the cell level) and long cycle life (>500 cycles with 80% capacity retention). To address this, future research should prioritize the following areas:

Cathode Design: Develop multifunctional hosts with high electronic conductivity, fast Li^+ transport, and efficient polysulfide confinement. For high sulfur loadings (>5 mg cm^{-2}), design architectures with controlled porosity and advanced binders that minimize inactive

DOI: 10.31635/ccschem.025.202506213
Citation: *CCS Chem.* **2025**, 7, 3235–3258
Link to VoR: https://doi.org/10.31635/ccschem.025.202506213

content while preserving mechanical integrity. Crucially, performance metrics should be evaluated under realistic conditions—high sulfur loading and lean electrolyte usage (E/S <3 μL mg^{-1}).

Electrolyte Engineering: Employ integrated designs that balance polysulfide solubility and stabilize the SEI on the LMA. Tailoring solvation structures and elucidating composition–property relationships will be key to enhancing redox kinetics and interfacial stability.

Lithium Metal Protection: Robust, scalable strategies are needed to support low N/P ratio operation while ensuring long-term cycling stability. These approaches should ensure uniform lithium deposition, suppress parasitic side reactions with polysulfides, and achieve Coulombic efficiencies >99% under practical conditions.

Solid-State Battery Development: Realizing practical ASSLSBs requires breakthroughs in cathode–electrolyte interfacial stability and redox kinetics. Solid electrolytes should combine high ionic conductivity with chemical and electrochemical stability. For lithium metal, approaches such as lightweight alloying and conductive frameworks with low tortuosity may mitigate dendrite growth and volume changes. Additionally, dry electrode processing and innovative cell designs will be vital to enable scalable, high-performance ASSLSBs for next-generation electric vehicles, drones, and other emerging technologies.

Conflict of Interest

There is no conflict of interest to report.

Funding Information

This work was supported by the National Key Research and Development Program of China (grant no. 2021YFB2500200), the National Natural Science Foundation of China (grant nos. 92372115 and 22409006), and the Beijing Natural Science Foundation (grant no. Z220020).

References

1. Lu, J.; Chen, Z. H.; Ma, Z. F.; Pan, F.; Curtiss, L. A.; Amine, K. The Role of Nanotechnology in the Development of Battery Materials for Electric Vehicles. *Nat. Nanotechnol.* **2016**, *11*, 1031–1038.
2. Zhou, G.; Chen, H.; Cui, Y. Formulating Energy Density for Designing Practical Lithium–Sulfur Batteries. *Nat. Energy* **2022**, *7*, 312–319.
3. Pang, Q.; Liang, X.; Kwok, C. Y.; Nazar, L. F. Advances in Lithium–Sulfur Batteries Based on Multifunctional Cathodes and Electrolytes. *Nat. Energy* **2016**, *1*, 16132.
4. Bruce, P. G.; Freunberger, S. A.; Hardwick, L. J.; Tarascon, J.-M. Li-O_2 and Li-S Batteries with High Energy Storage. *Nat. Mater.* **2012**, *11*, 19–29.
5. Herbert, D.; Ulam, J. Electric Dry Cells and Storage Batteries. US Patent US3043896, **1962**.
6. Ji, X. L.; Lee, K. T.; Nazar, L. F. A Highly Ordered Nanostructured Carbon-Sulphur Cathode for Lithium-Sulphur Batteries. *Nat. Mater.* **2009**, *8*, 500–506.
7. Zhao, C.; Xu, G.-L.; Yu, Z.; Zhang, L.; Hwang, I.; Mo, Y.-X.; Ren, Y.; Cheng, L.; Sun, C.-J.; Ren, Y.; Zuo, X.; Li, J.-T.; Sun, S.-G.; Amine, K.; Zhao, T. A High-Energy and Long-Cycling Lithium–Sulfur Pouch Cell via a Macroporous Catalytic Cathode with Double-End Binding Sites. *Nat. Nanotechnol.* **2020**, *16*, 166–173.
8. Gu, Q.; Lu, M.; Cao, Y.; Zhang, B. Revealing the Catalytic Conversion via in Situ Characterization for Lithium–Sulfur Batteries. *Renewables* **2023**, *1*, 601–621.
9. Pang, Q.; Shyamsunder, A.; Narayanan, B.; Kwok, C. Y.; Curtiss, L. A.; Nazar, L. F. Tuning the Electrolyte Network Structure to Invoke Quasi-Solid State Sulfur Conversion and Suppress Lithium Dendrite Formation in Li-S Batteries. *Nat. Energy* **2018**, *3*, 783–791.
10. Liu, L.; Yin, Y. X.; Li, J. Y.; Wang, S. H.; Guo, Y. G.; Wan, L. J. Uniform Lithium Nucleation/Growth Induced by Lightweight Nitrogen-Doped Graphitic Carbon Foams for High-Performance Lithium Metal Anodes. *Adv. Mater.* **2018**, *30*, 1706216.
11. Yang, X.; Li, X.; Adair, K.; Zhang, H.; Sun, X. Structural Design of Lithium–Sulfur Batteries: From Fundamental Research to Practical Application. *Electrochem. Energy Rev.* **2018**, *1*, 239–293.
12. Feng, J.; Liu, T.; Li, H.; Hu, Y.-S.; Mao, H.; Suo, L. Ultralight Electrolyte with Protective Encapsulation Solvation Structure Enables Hybrid Sulfur-Based Primary Batteries Exceeding 660 Wh/Kg. *J. Am. Chem. Soc.* **2024**, *146*, 3755–3763.
13. Cheng, Q.; Chen, Z.-X.; Li, X.-Y.; Hou, L.-P.; Bi, C.-X.; Zhang, X.-Q.; Huang, J.-Q.; Li, B.-Q. Constructing a 700 Wh Kg^{-1}-Level Rechargeable Lithium-Sulfur Pouch Cell. *J. Energy Chem.* **2023**, *76*, 181–186.
14. Zhou, G.; Tian, H.; Jin, Y.; Tao, X.; Liu, B.; Zhang, R.; Seh, Z. W.; Zhuo, D.; Liu, Y.; Sun, J.; Zhao, J.; Zu, C.; Wu, D. S.; Zhang, Q.; Cui, Y. Catalytic Oxidation of Li_2S on the Surface of Metal Sulfides for Li-S Batteries. *Proc. Natl. Acad. Sci. USA* **2017**, *114*, 840–845.
15. Fang, R.; Zhao, S.; Sun, Z.; Wang, D.-W.; Cheng, H.-M.; Li, F. More Reliable Lithium-Sulfur Batteries: Status, Solutions and Prospects. *Adv. Mater.* **2017**, *29*, 1606823.
16. Zhang, S.; Ueno, K.; Dokko, K.; Watanabe, M. Recent Advances in Electrolytes for Lithium-Sulfur Batteries. *Adv. Energy Mater.* **2015**, *5*, 1500117.
17. Li, Z.; Sami, I.; Yang, J.; Li, J.; Kumar, R. V.; Chhowalla, M. Lithiated Metallic Molybdenum Disulfide Nanosheets for High-Performance Lithium-Sulfur Batteries. *Nat. Energy* **2023**, *8*, 84–93.
18. Li, M.; Liu, H.; Cheng, Z.; He, J.; Li, H.; Zhang, L.; Liu, T.; Wang, X.; Wang, P.; Liu, Z.; Cui, G. Atomic-Level Modulation of Imine and Cobalt Enables a Homogeneous $Co_{5.47}N$ Catalyst for High-Performance Lithium-Sulfur Batteries. *Adv. Energy Mater.* **2025**, *15*, 2405766.
19. Xie, Y.; Pan, G.; Jin, Q.; Qi, X.; Wang, T.; Li, W.; Xu, H.; Zheng, Y.; Li, S.; Qie, L.; Huang, Y.; Li, J. Semi-Flooded Sulfur

DOI: 10.31635/ccschem.025.202506213
Citation: *CCS Chem.* **2025**, 7, 3235–3258
Link to VoR: https://doi.org/10.31635/ccschem.025.202506213

Cathode with Ultralean Absorbed Electrolyte in Li-S Battery. *Adv. Sci.* **2020**, *7*, 1903168.
20. Li, H.; Feng, J.; Liu, T.; Qin, K.; Zhu, X.; Suo, L. Suppressing Sulfur Crosstalk Lowers the Bar of Lithium Metal Anode for Practical Li-S Pouch Cells. *Energy Storage Mater.* **2024**, *71*, 103664.
21. Han, Z.; Chen, A.; Li, Z.; Zhang, M.; Wang, Z.; Yang, L.; Gao, R.; Jia, Y.; Ji, G.; Lao, Z.; Xiao, X.; Tao, K.; Gao, J.; Lv, W.; Wang, T.; Li, J.; Zhou, G. Machine Learning-Based Design of Electrocatalytic Materials Towards High-Energy Lithium|| Sulfur Batteries Development. *Nat. Commun.* **2024**, *15*, 8433.
22. Cheng, Q.; Chen, Z. X.; Li, X. Y.; Bi, C. X.; Sun, F.; Zhang, X. Q.; Ma, X.; Li, B. Q.; Huang, J. Q. Deciphering the Degradation Mechanism of High-Rate and High-Energy-Density Lithium–Sulfur Pouch Cells. *Adv. Energy Mater.* **2023**, *13*, 2301770.
23. Huang, Z.; Liang, Y.; Wu, Z.; Kong, Y.; Bai, M.; Li, M.; Hong, B.; Huang, T.; Huang, S.; Chen, H.; Zhang, S. Multifunctional Ultrathin $Ti_3C_2T_x$ Mxene@$CuCO_2O_4$ /Pe Separator for Ultra-High-Energy-Density and Large-Capacity Lithium-Sulfur Pouch Cells. *Adv. Mater.* **2024**, *37*, 2410318.
24. Li, X.-Y.; Feng, S.; Zhao, C.-X.; Cheng, Q.; Chen, Z.-X.; Sun, S.-Y.; Chen, X.; Zhang, X.-Q.; Li, B.-Q.; Huang, J.-Q.; Zhang, Q. Regulating Lithium Salt to Inhibit Surface Gelation on an Electrocatalyst for High-Energy-Density Lithium-Sulfur Batteries. *J. Am. Chem. Soc.* **2022**, *144*, 14638–14646.
25. Lin, Y.; Zhou, Y.; Huang, S.; Xiao, M.; Han, D.; Qin, J.; Wang, S.; Meng, Y. Catalytic Disproportionation for Suppressing Polysulfide Shuttle in Li–S Pouch Cells: Beyond Adsorption Interactions. *Adv. Energy Mater.* **2022**, *12*, 2201912.
26. Han, Z.; Gao, R.; Wang, T.; Tao, S.; Jia, Y.; Lao, Z.; Zhang, M.; Zhou, J.; Li, C.; Piao, Z.; Zhang, X.; Zhou, G. Machine-Learning-Assisted Design of a Binary Descriptor to Decipher Electronic and Structural Effects on Sulfur Reduction Kinetics. *Nat. Catal.* **2023**, *6*, 1073–1086.
27. Kim, S.; Lim, W.-G.; Jung, H.; Jeong, Y. C.; Park, C.-Y.; Yang, S. B.; Lee, C. H.; Wang, D.; Sohn, K.; Han, J. W.; Lee, J. Protective Catalytic Layer Powering Activity and Stability of Electrocatalyst for High-Energy Lithium-Sulfur Pouch Cell. *Nat. Commun.* **2025**, *16*, 1649.
28. Su, L. L.; Yao, N.; Li, Z.; Bi, C. X.; Chen, Z. X.; Chen, X.; Li, B. Q.; Zhang, X. Q.; Huang, J. Q. Improving Rate Performance of Encapsulating Lithium-Polysulfide Electrolytes for Practical Lithium-Sulfur Batteries. *Angew. Chem. Int. Ed.* **2024**, *63*, e202318785.
29. Sun, W.; Liu, S.; Li, Y.; Wang, D.; Guo, Q.; Hong, X.; Xie, K.; Ma, Z.; Zheng, C.; Xiong, S. Monodispersed FeS_2 Electrocatalyst Anchored to Nitrogen-Doped Carbon Host for Lithium–Sulfur Batteries. *Adv. Funct. Mater.* **2022**, *32*, 2205471.
30. Yang, Z.; Yan, R.; Han, J.; Wu, T.; Wu, Q.; Wei, G.; Fu, Y.; Wen, M. Oxygen Bridges of $CoTe_2$/Co–O–NC Enhancing Adsorption-Catalysis of Polysulfide for Stable Lithium–Sulfur Batteries. *Adv. Funct. Mater.* **2025**, *35*, 2417834.
31. Xue, W.; Shi, Z.; Suo, L.; Wang, C.; Wang, Z.; Wang, H.; So, K. P.; Maurano, A.; Yu, D.; Chen, Y.; Qie, L.; Zhu, Z.; Xu, G.; Kong, J.; Li, J. Intercalation-Conversion Hybrid Cathodes Enabling Li-S Full-Cell Architectures with Jointly Superior Gravimetric and Volumetric Energy Densities. *Nat. Energy* **2019**, *4*, 374–382.
32. Yao, W.; Xu, J.; Cao, Y.; Meng, Y.; Wu, Z.; Zhan, L.; Wang, Y.; Zhang, Y.; Manke, I.; Chen, N.; Yang, C.; Chen, R. Dynamic Intercalation–Conversion Site Supported Ultrathin 2D Mesoporous SnO_2/$SnSe_2$ Hybrid as Bifunctional Polysulfide Immobilizer and Lithium Regulator for Lithium-Sulfur Chemistry. *ACS Nano* **2022**, *16*, 10783–10797.
33. Zhao, Z.; Pan, Y.; Yi, S.; Su, Z.; Chen, H.; Huang, Y.; Niu, B.; Long, D.; Zhang, Y. Enhanced Electron Delocalization Within Coherent Nano-Heterocrystal Ensembles for Optimizing Polysulfide Conversion in High-Energy-Density Li-S Batteries. *Adv. Mater.* **2023**, *36*, 2310052.
34. Song, Y.-W.; Shen, L.; Yao, N.; Li, X.-Y.; Bi, C.-X.; Li, Z.; Zhou, M.-Y.; Zhang, X.-Q.; Chen, X.; Li, B.-Q.; Huang, J.-Q.; Zhang, Q. Cationic Lithium Polysulfides in Lithium-Sulfur Batteries. *Chem* **2022**, *8*, 3031–3050.
35. Zhao, C. X.; Li, X. Y.; Zhao, M.; Chen, Z. X.; Song, Y. W.; Chen, W. J.; Liu, J. N.; Wang, B.; Zhang, X. Q.; Chen, C. M.; Li, B. Q.; Huang, J. Q.; Zhang, Q. Semi-Immobilized Molecular Electrocatalysts for High-Performance Lithium-Sulfur Batteries. *J. Am. Chem. Soc.* **2021**, *143*, 19865–19872.
36. Cheng, H.; Zhang, S.; Li, S.; Gao, C.; Zhao, S.; Lu, Y.; Wang, M. Engineering Fe and V Coordinated Bimetallic Oxide Nanocatalyst Enables Enhanced Polysulfides Mediation for High Energy Density Li-S Battery. *Small* **2022**, *18*, e2202557.
37. Liu, Y.; An, Y.; Fang, C.; Ye, Y.; An, Y.; He, M.; Jia, Y.; Hong, X.; Liu, Y.; Gao, S.; Hao, Y.; Chen, J.; Zheng, J.; Lu, Y.; Zou, R.; Pang, Q. Surface-Localized Phase Mediation Accelerates Quasi-Solid-State Reaction Kinetics in Sulfur Batteries. *Nat. Chem.* **2025**, *17*, 614–623.
38. Lim, W. G.; Park, C. Y.; Jung, H.; Kim, S.; Kang, S. H.; Lee, Y. G.; Jeong, Y. C.; Yang, S. B.; Sohn, K.; Han, J. W.; Lee, J. Cooperative Electronic Structure Modulator of Fe Single-Atom Electrocatalyst for High Energy and Long Cycle Li-S Pouch Cell. *Adv. Mater.* **2023**, *35*, 2208999.
39. Shi, L.; Bak, S.-M.; Shadike, Z.; Wang, C.; Niu, C.; Northrup, P.; Lee, H.; Baranovskiy, A. Y.; Anderson, C. S.; Qin, J.; Feng, S.; Ren, X.; Liu, D.; Yang, X.-Q.; Gao, F.; Lu, D.; Xiao, J.; Liu, J. Reaction Heterogeneity in Practical High-Energy Lithium-Sulfur Pouch Cells. *Energy Environ. Sci.* **2020**, *13*, 3620–3632.
40. He, M.; Zhu, L.; Liu, Y.; Jia, Y.; Hao, Y.; Ye, G.; Hong, X.; Xiao, Z.; Ma, Y.; Chen, J.; Shafqat, M. B.; Pang, Q. Highly Solvating Electrolytes with Core-Shell Solvation Structure for Lean-Electrolyte Lithium-Sulfur Batteries. *Angew. Chem. Int. Ed.* **2024**, *64*, e202415053.
41. Kong, L.; Jin, Q.; Huang, J.-Q.; Zhao, L.-D.; Li, P.; Li, B.-Q.; Peng, H.-J.; Zhang, X.; Zhang, Q. Nonuniform Redistribution of Sulfur and Lithium Upon Cycling: Probing the Origin of Capacity Fading in Lithium–Sulfur Pouch Cells. *Energy Technol.* **2019**, *7*, 1900111.
42. Fei, Y.; Li, G. Unveiling the Pivotal Parameters for Advancing High Energy Density in Lithium-Sulfur Batteries: A Comprehensive Review. *Adv. Funct. Mater.* **2024**, *34*, 2312550.

DOI: 10.31635/ccschem.025.202506213
Citation: *CCS Chem.* **2025**, 7, 3235–3258
Link to VoR: https://doi.org/10.31635/ccschem.025.202506213

43. Luo, D.; Chen, H.; Liu, G.; Nie, Y.; Yang, T.; Ma, Q.; Lai, X.; Li, J.; Cui, Y.; Wang, X.; Zhang, Y.; Chen, Z. Constructing Abnormal Step-Scheme Nano-Heterointerfaces as Sulfur Electrocatalysts with Desirable Electron Confinement for Practical Li-S Battery. *Renewables* **2024**, *2*, 61–72.
44. Cai, G.; Lv, H.; Zhang, G.; Liu, D.; Zhang, J.; Zhu, J.; Xu, J.; Kong, X.; Jin, S.; Wu, X.; Ji, H. A Volcano Correlation Between Catalytic Activity for Sulfur Reduction Reaction and Fe Atom Count in Metal Center. *J. Am. Chem. Soc.* **2024**, *146*, 13055–13065.
45. Liu, R.; Wei, Z.; Peng, L.; Zhang, L.; Zohar, A.; Schoeppner, R.; Wang, P.; Wan, C.; Zhu, D.; Liu, H.; Wang, Z.; Tolbert, S. H.; Dunn, B.; Huang, Y.; Sautet, P.; Duan, X. Establishing Reaction Networks in the 16-Electron Sulfur Reduction Reaction. *Nature* **2024**, *626*, 98–104.
46. Zhou, S.; Shi, J.; Liu, S.; Li, G.; Pei, F.; Chen, Y.; Deng, J.; Zheng, Q.; Li, J.; Zhao, C.; Hwang, I.; Sun, C.-J.; Liu, Y.; Deng, Y.; Huang, L.; Qiao, Y.; Xu, G.-L.; Chen, J.-F.; Amine, K.; Sun, S.-G.; Liao, H.-G. Visualizing Interfacial Collective Reaction Behaviour of Li-S Batteries. *Nature* **2023**, *621*, 75–81.
47. Baek, M.; Shin, H.; Char, K.; Choi, J. W. New High Donor Electrolyte for Lithium-Sulfur Batteries. *Adv. Mater.* **2020**, *32*, 2005022.
48. Gupta, A.; Bhargav, A.; Manthiram, A. Highly Solvating Electrolytes for Lithium-Sulfur Batteries. *Adv. Energy Mater.* **2019**, *9*, 1803096.
49. He, Q.; Gorlin, Y.; Patel, M. U. M.; Gasteiger, H. A.; Lu, Y.-C. Unraveling the Correlation Between Solvent Properties and Sulfur Redox Behavior in Lithium Sulfur Batteries. *J. Electrochem. Soc.* **2018**, *165*, A4027–A4033.
50. Zhang, G.; Peng, H. J.; Zhao, C. Z.; Chen, X.; Zhao, L. D.; Li, P.; Huang, J. Q.; Zhang, Q. The Radical Pathway Based on Alithium-Metal-Compatible Highdielectric Electrolyte for Lithium–Sulfur Batteries. *Angew. Chem. Int. Ed.* **2018**, *57*, 16732–16736.
51. Li, Z. J.; Zhou, Y. C.; Wang, Y.; Lu, Y. C. Solvent-Mediated Li_2S Electrodeposition: A Critical Manipulator in Lithium-Sulfur Batteries. *Adv. Energy Mater.* **2019**, *9*, 1802207.
52. Elabd, A.; Kim, J.; Sethio, D.; Kang, S.; Kang, T.; Choi, J. W.; Coskun, A. Dual Functional High Donor Electrolytes for Lithium–Sulfur Batteries Under Lithium Nitrate Free and Lean Electrolyte Conditions. *ACS Energy Lett.* **2022**, *7*, 2459–2468.
53. Zhong, N.; Lei, C.; Meng, R.; Li, J.; He, X.; Liang, X. Electrolyte Solvation Chemistry for the Solution of High-Donor-Number Solvent for Stable Li-S Batteries. *Small* **2022**, *18*, 2200046.
54. Cheng, Q.; Xu, W. H.; Qin, S. Y.; Das, S.; Jin, T. W.; Li, A. J.; Li, A. C.; Qie, B. Y.; Yao, P. C.; Zhai, H. W.; Shi, C. M.; Yong, X.; Yang, Y. Full Dissolution of Li_2S_8 to Li_2S in Safe Eutectic Solvent for Rechargeable Lithium-Sulfur Batteries. *Angew. Chem. Int. Ed.* **2019**, *58*, 5557–5561.
55. Chu, H.; Noh, H.; Kim, Y. J.; Yuk, S.; Lee, J. H.; Lee, J.; Kwack, H.; Kim, Y.; Yang, D. K.; Kim, H. T. Achieving Three-Dimensional Lithium Sulfide Growth in Lithium-Sulfur Batteries Using High-Donor-Number Anions. *Nat. Commun.* **2019**, *10*, 188.
56. Chu, H.; Jung, J.; Noh, H.; Yuk, S.; Lee, J.; Lee, J. H.; Baek, J.; Roh, Y.; Kwon, H.; Choi, D.; Sohn, K.; Kim, Y.; Kim, H. T. Unraveling the Dual Functionality of High-Donor-Number Anion in Lean-Electrolyte Lithium-Sulfur Batteries. *Adv. Energy Mater.* **2020**, *10*, 2000493.
57. Gupta, A.; Bhargav, A.; Manthiram, A. Evoking High-Donor-Number-Assisted and Organosulfur-Mediated Conversion in Lithium-Sulfur Batteries. *ACS Energy Lett.* **2020**, *6*, 224–231.
58. Song, Y. W.; Shen, L.; Yao, N.; Feng, S.; Cheng, Q.; Ma, J.; Chen, X.; Li, B. Q.; Zhang, Q. Anion-Involved Solvation Structure of Lithium Polysulfides in Lithium-Sulfur Batteries. *Angew. Chem. Int. Ed.* **2024**, *63*, e202400343.
59. He, M.; An, Y.; Zhu, L.; Liu, Y.; Jia, Y.; Hao, Y.; Ye, G.; Hong, X.; Xiao, Z.; Ma, Y.; Song, H.; Shen, K.; Yan, Y.; Shi, W.; Zheng, C.; Chen, J.; Shafqat, M. B.; Pang, Q. Regulating Polysulfide Clustering with an Anion Acceptor for Low-Temperature Sulfur Batteries. *Nano Lett.* **2025**, *25*, 3029–3037.
60. Zhang, W.; Zhu, J.; Ye, Y.; She, J.; Kong, X.; Jin, S.; Peng, Z.; Ji, H. Suppressing Shuttle Effect via Cobalt Phthalocyanine Mediated Dissociation of Lithium Polysulfides for Enhanced Li-S Battery Performance. *Adv. Funct. Mater.* **2024**, *34*, 2403888.
61. Deng, T.; Wang, J.; Zhao, H.; Jin, Z.; Jin, L.; Men, X.; Wang, J.; Liu, Y.; Tang, W.; Abdelkader, A. M.; Kumar, R. V.; Ding, S.; Fu, Y.; Xi, K. Dynamically Regulating Polysulfide Degradation via Organic Sulfur Electrolyte Additives in Lithium-Sulfur Batteries. *Adv. Energy Mater.* **2024**, *14*, 2402319.
62. Unemoto, A.; Ogawa, H.; Gambe, Y.; Honma, I. Development of Lithium-Sulfur Batteries Using Room Temperature Ionic Liquid-Based Quasi-Solid-State Electrolytes. *Electrochim. Acta* **2014**, *125*, 386–394.
63. Dokko, K.; Tachikawa, N.; Yamauchi, K.; Tsuchiya, M.; Yamazaki, A.; Takashima, E.; Park, J.-W.; Ueno, K.; Seki, S.; Serizawa, N.; Watanabe, M. Solvate Ionic Liquid Electrolyte for Li-S Batteries. *J. Electrochem. Soc.* **2013**, *160*, A1304–A1310.
64. Lee, C. W.; Pang, Q.; Ha, S.; Cheng, L.; Han, S. D.; Zavadil, K. R.; Gallagher, K. G.; Nazar, L. F.; Balasubramanian, M. Directing the Lithium-Sulfur Reaction Pathway via Sparingly Solvating Electrolytes for High Energy Density Batteries. *ACS Cent. Sci.* **2017**, *3*, 605–613.
65. Su, C. C.; He, M.; Amine, R.; Amine, K. A Selection Rule for Hydrofluoroether Electrolyte Cosolvent: Establishing a Linear Free-Energy Relationship in Lithium-Sulfur Batteries. *Angew. Chem. Int. Ed.* **2019**, *58*, 10591–10595.
66. Liao, K.; Pai, M. H.; Manthiram, A. Tuning the Solvation Structure of a Weakly Solvating Cyclic Ether Electrolyte for Wide-Temperature Cycling of Lithium-Sulfurized Polyacrylonitrile Batteries. *Adv. Energy Mater.* **2024**, *15*, 2403733.
67. Liu, Y.; Xu, L.; Yu, Y.; He, M.; Zhang, H.; Tang, Y.; Xiong, F.; Gao, S.; Li, A.; Wang, J.; Xu, S.; Aurbach, D.; Zou, R.; Pang, Q. Stabilized Li-S Batteries with Anti-Solvent-Tamed Quasi-Solid-State Reaction. *Joule* **2023**, *7*, 2074–2091.
68. Han, Z.; Li, S.; Sun, M.; He, R.; Zhong, W.; Yu, C.; Cheng, S.; Xie, J. Fluorobenzene Diluted Low-Density Electrolyte for

DOI: 10.31635/ccschem.025.202506213
Citation: *CCS Chem.* **2025**, 7, 3235–3258
Link to VoR: https://doi.org/10.31635/ccschem.025.202506213

High-Energy Density and High-Performance Lithium-Sulfur Batteries. *J. Energy Chem.* **2022**, *68*, 752–761.
69. Cheng, H.; Zhang, S.; Zhang, B.; Lu, Y. n-Hexane Diluted Electrolyte with Ultralow Density Enables Li-S Pouch Battery Toward >400 Wh kg^{-1}. *Small* **2022**, *19*, 2206375.
70. Kim, I.; Kim, S.; Cho, H.; Jung, J.; Kwon, H.; Kim, D.; Shin, Y.; Kim, H. T. Moderately Solvating Electrolyte with Fluorinated Cosolvents for Lean-Electrolyte Li-S Batteries. *Adv. Energy Mater.* **2024**, *15*, 2403828.
71. Li, Z.; Hou, L. P.; Yao, N.; Li, X. Y.; Chen, Z. X.; Chen, X.; Zhang, X. Q.; Li, B. Q.; Zhang, Q. Correlating Polysulfide Solvation Structure with Electrode Kinetics Towards Long-Cycling Lithium-Sulfur Batteries. *Angew. Chem. Int. Ed.* **2023**, *62*, e202309968.
72. Hou, L.-P.; Zhang, X.-Q.; Yao, N.; Chen, X.; Li, B.-Q.; Shi, P.; Jin, C.-B.; Huang, J.-Q.; Zhang, Q. An Encapsulating Lithium-Polysulfide Electrolyte for Practical Lithium-Sulfur Batteries. *Chem* **2022**, *8*, 1083–1098.
73. Li, X.-Y.; Feng, S.; Song, Y.-W.; Zhao, C.-X.; Li, Z.; Chen, Z.-X.; Cheng, Q.; Chen, X.; Zhang, X.-Q.; Li, B.-Q.; Huang, J.-Q.; Zhang, Q. Kinetic Evaluation on Lithium Polysulfide in Weakly Solvating Electrolyte Toward Practical Lithium-Sulfur Batteries. *J. Am. Chem. Soc.* **2024**, *146*, 14754–14764.
74. Li, X.-Y.; Li, B.-Q.; Feng, S.; Li, Z.; Shen, L.; Sun, S.-Y.; Chen, Z.-X.; Jin, T.; Chen, X.; Zhao, M.; Zhang, X.-Q.; Huang, J.-Q.; Zhang, Q. Two-Stage Solvation of Lithium Polysulfides in Working Lithium-Sulfur Batteries. *J. Am. Chem. Soc.* **2025**, *147*, 15435–15447.
75. Jin, T.; Li, X. Y.; Zhao, M.; Feng, S.; Li, Z.; Chen, Z. X.; Peng, H. J.; Li, B. Q.; Huang, J. Q. Promoting the Rate Performances of Weakly Solvating Electrolyte-Based Lithium-Sulfur Batteries. *Angew. Chem. Int. Ed.* **2025**, *64*, e202504898.
76. Su, L.-L.; Wu, M.-X.; Sun, S.-Y.; Bi, C.-X.; Zheng, Z.; Zhao, M.; Li, B.-Q.; Zhang, X.-Q.; Huang, J.-Q. Long-Cycling Lithium-Sulfur Batteries Enabled by Reactivating Inactive Lithium. *ACS Energy Lett.* **2024**, *10*, 313–319.
77. Hou, L. P.; Li, Y.; Li, Z.; Zhang, Q. K.; Li, B. Q.; Bi, C. X.; Chen, Z. X.; Su, L. L.; Huang, J. Q.; Wen, R.; Zhang, X. Q.; Zhang, Q. Electrolyte Design for Improving Mechanical Stability of Solid Electrolyte Interphase in Lithium-Sulfur Batteries. *Angew. Chem. Int. Ed.* **2023**, *62*, e202305466.
78. Liu, F.; Xu, D.; Liu, Z.; Wang, L.; Chen, M.; Zhou, D.; Xiao, Z. Potassium 3-Thiophenetrifluoroborate Based Preferential Redox Toward Highly Efficient Bilateral Protection for Full Li-S Batteries. *Adv. Funct. Mater.* **2024**, *35*, 2412923.
79. Zhao, Y.; Huang, L.; Zhao, D.; Yang Lee, J. Fast Polysulfide Conversion Catalysis and Reversible Anode Operation by a Single Cathode Modifier in Li-Metal Anode-Free Lithium-Sulfur Batteries. *Angew. Chem. Int. Ed.* **2023**, *62*, e202308976.
80. Luo, Y.; Zhang, C.; Cai, J.; Wei, Z.; Huang, Q.; Zheng, Z. Understanding and Passivation of Surface Corrosion of Cu for Stable Low-N/P-Ratio Lithium-Sulfur Battery. *Adv. Funct. Mater.* **2024**, *35*, 2418043.
81. Lv, S.; Ma, X.; Ke, S.; Wang, Y.; Ma, T.; Yuan, S.; Jin, Z.; Zuo, J.-L. Metal-Coordinated Covalent Organic Frameworks as Advanced Bifunctional Hosts for Both Sulfur Cathodes and Lithium Anodes in Lithium-Sulfur Batteries. *J. Am. Chem. Soc.* **2024**, *146*, 9385–9394.
82. Kim, J. T.; Su, H.; Zhong, Y.; Wang, C.; Wu, H.; Zhao, D.; Wang, C.; Sun, X.; Li, Y. All-Solid-State Lithium-Sulfur Batteries Through a Reaction Engineering Lens. *Nat. Chem. Eng.* **2024**, *1*, 400–410.
83. Amici, J.; Asinari, P.; Ayerbe, E.; Barboux, P.; Bayle-Guillemaud, P.; Behm, R. J.; Berecibar, M.; Berg, E.; Bhowmik, A.; Bodoardo, S.; Castelli, I. E.; Cekic-Laskovic, I.; Christensen, R.; Clark, S.; Diehm, R.; Dominko, R.; Fichtner, M.; Franco, A. A.; Grimaud, A.; Guillet, N.; Hahlin, M.; Hartmann, S.; Heiries, V.; Hermansson, K.; Heuer, A.; Jana, S.; Jabbour, L.; Kallo, J.; Latz, A.; Lorrmann, H.; Lovvik, O. M.; Lyonnard, S.; Meeus, M.; Paillard, E.; Perraud, S.; Placke, T.; Punckt, C.; Raccurt, O.; Ruhland, J.; Sheridan, E.; Stein, H.; Tarascon, J. M.; Trapp, V.; Vegge, T.; Weil, M.; Wenzel, W.; Winter, M.; Wolf, A.; Edström, K. A Roadmap for Transforming Research to Invent the Batteries of the Future Designed Within the European Large Scale Research Initiative Battery 2030+. *Adv. Energy Mater.* **2022**, *12*, 2102785.
84. Lu, Y.; Rong, X.; Hu, Y.-S.; Chen, L.; Li, H. Research and Development of Advanced Battery Materials in China. *Energy Storage Mater.* **2019**, *23*, 144–153.
85. Bresser, D.; Hosoi, K.; Howell, D.; Li, H.; Zeisel, H.; Amine, K.; Passerini, S. Perspectives of Automotive Battery R&D in China, Germany, Japan, and the USA. *J. Power Sources* **2018**, *382*, 176–178.
86. Wu, J.; Liu, S.; Han, F.; Yao, X.; Wang, C. Lithium/Sulfide All-Solid-State Batteries Using Sulfide Electrolytes. *Adv. Mater.* **2021**, *33*, 2000751.
87. Chen, Z.; Liang, Z.; Zhong, H.; Su, Y.; Wang, K.; Yang, Y. Bulk/Interfacial Synergetic Approaches Enable the Stable Anode for High Energy Density All-Solid-State Lithium–Sulfur Batteries. *ACS Energy Lett.* **2022**, *7*, 2761–2770.
88. Yao, X.; Huang, N.; Han, F.; Zhang, Q.; Wan, H.; Mwizerwa, J. P.; Wang, C.; Xu, X. High-Performance All-Solid-State Lithium-Sulfur Batteries Enabled by Amorphous Sulfur-Coated Reduced Graphene Oxide Cathodes. *Adv. Energy Mater.* **2017**, *7*, 1602923.
89. Yang, X.; Luo, J.; Sun, X. Towards High-Performance Solid-State Li-S Batteries: From Fundamental Understanding to Engineering Design. *Chem. Soc. Rev.* **2020**, *49*, 2140–2195.
90. Zhang, Y.; Liu, T.; Zhang, Q.; Zhang, X.; Wang, S.; Wang, X.; Li, L.; Fan, L.-Z.; Nan, C.-W.; Shen, Y. High-Performance All-Solid-State Lithium-Sulfur Batteries with Sulfur/Carbon Nano-Hybrids in a Composite Cathode. *J. Mater. Chem. A* **2018**, *6*, 23345–23356.
91. Sun, X.; Li, Q.; Cao, D.; Wang, Y.; Anderson, A.; Zhu, H. High Surface Area N-Doped Carbon Fibers with Accessible Reaction Sites for All-Solid-State Lithium-Sulfur Batteries. *Small* **2022**, *18*, 2105678.
92. Xu, G.; Yan, Z.; Yang, H.; Zhang, X.; Su, Y.; Huang, Z.; Zhang, L.; Tang, Y.; Wang, Z.; Zhu, L. Multiscale Structural Engineering of Sulfur/Carbon Cathodes Enables High Performance All-Solid-State Li-S Batteries. *Small* **2023**, *19*, 2300420.

DOI: 10.31635/ccschem.025.202506213
Citation: *CCS Chem.* **2025**, 7, 3235–3258
Link to VoR: https://doi.org/10.31635/ccschem.025.202506213

93. Luo, Y.; Pan, S.; Tian, J.; Liang, Y.; Zhong, H.; Ma, R.; Gu, J.; Wu, Y.; Zhang, H.; Lin, H. Engineering Triple-Phase Interfaces with Hierarchical Carbon Nanocages for High-Areal-Capacity All-Solid-State Li-S Batteries. *Adv. Mater.* **2024**, *36*, 2413325.
94. Li, X.; Liang, J.; Luo, J.; Wang, C.; Li, X.; Sun, Q.; Li, R.; Zhang, L.; Yang, R.; Lu, S. High-Performance Li-SeS_x All-Solid-State Lithium Batteries. *Adv. Mater.* **2019**, *31*, 1808100.
95. Zhou, J.; Holekevi Chandrappa, M. L.; Tan, S.; Wang, S.; Wu, C.; Nguyen, H.; Wang, C.; Liu, H.; Yu, S.; Miller, Q. R. Healable and Conductive Sulfur Iodide for Solid-State Li-S Batteries. *Nature* **2024**, *627*, 301–305.
96. Whang, G.; Ketter, L.; Zhao, T.; Nazmutdinova, E.; Kraft, M. A.; Zeier, W. G. High Areal Capacity Cation and Anionic Redox Solid-State Batteries Enabled by Transition Metal Sulfide Conversion. *ACS Appl. Mater. Interfaces* **2024**, *16*, 42189–42197.
97. Zhong, H.; Su, Y.; Ma, R.; Luo, Y.; Lin, H.; Gu, J.; Gong, Z.; Yang, Y. Nano-Scale Interface Engineering of Sulfur Cathode to Enable High-Performance All-Solid-State Li-S Batteries. *Adv. Funct. Mater.* **2024**, *34*, 2315925.
98. Wang, M.; Su, H.; Zhong, Y.; Zhou, C.; Chen, G.; Wang, X.; Tu, J. A Unitized Encapsulation Architecture with Durable Epitaxial Ion-Conductive Scaffolds for Ultrastable Solid-State Sulfur Cathode. *Energy Environ. Sci.* **2025**, *18*, 4162–4175.
99. Yu, Z.; Singh, B.; Yu, Y.; Nazar, L. F. Suppressing Argyrodite Oxidation by Tuning the Host Structure for High-Areal-Capacity All-Solid-State Lithium-Sulfur Batteries. *Nat. Mater.* **2025**, *24*, 1082–1090.
100. Cao, D. X.; Zhang, Y. X.; Ji, T. T.; Zhao, X. H.; Cakmak, E.; Ozcan, S.; Geiwitz, M.; Bilheux, J.; Xu, K.; Wang, Y.; Burch, K. S.; Tu, Q. H.; Zhu, H. L. Li Dynamics in Mixed Ionic-Electronic Conducting Interlayer of All-Solid-State Li-Metal Batteries. *Nano Lett.* **2024**, *24*, 1544–1552.
101. Wang, D.; Gwalani, B.; Wierzbicki, D.; Singh, V.; Jhang, L.-J.; Rojas, T.; Kou, R.; Liao, M.; Ye, L.; Jiang, H. Overcoming the Conversion Reaction Limitation at Three-Phase Interfaces Using Mixed Conductors Towards Energy-Dense Solid-State Li-S Batteries. *Nat. Mater.* **2025**, *24*, 243–251.
102. Cui, L. F.; Zhang, S.; Ju, J. W.; Liu, T.; Zheng, Y.; Xu, J. H.; Wang, Y. T.; Li, J. D.; Zhao, J. W.; Ma, J.; Wang, J. Z.; Xu, G. J.; Chan, T. S.; Huang, Y. C.; Haw, S. C.; Chen, J. M.; Hu, Z. W.; Cui, G. L. A Cathode Homogenization Strategy for Enabling Long-Cycle-Life All-Solid-State Lithium Batteries. *Nat. Energy* **2024**, *9*, 1084–1094.
103. Liu, C.; Zhang, T.; Wang, R.; Chen, B.; Wang, D.; Wang, T.; Yang, Z.; Liu, T.; Mao, Q.; Li, T. Regulating P-Band Center of Sulfur in Li-Argyrodite to Stabilize Dual Solid-Solid Interface for Robust All-Solid-State Lithium-Sulfur Battery. *Adv. Funct. Mater.* **2025**, *35*, 2412144.
104. Cao, Y.; Geng, C.; Bai, C.; Peng, L.; Lan, J.; Liu, J.; Han, J.; Liu, B.; He, Y.; Kang, F. Integrating Solid Interfaces for Catalysis in All-Solid-State Lithium-Sulfur Batteries. *Energy Environ. Sci.* **2025**, *18*, 3795–3806.
105. Kim, J. T.; Rao, A.; Nie, H.-Y.; Hu, Y.; Li, W.; Zhao, F.; Deng, S.; Hao, X.; Fu, J.; Luo, J. Manipulating Li_2S_2/Li_2S Mixed Discharge Products of All-Solid-State Lithium Sulfur Batteries for Improved Cycle Life. *Nat. Commun.* **2023**, *14*, 6404.
106. Yu, P.; Sun, S.; Sun, C.; Zeng, C.; Hua, Z.; Ahmad, N.; Shao, R.; Yang, W. Active Regulation Volume Change of Micrometer-Size Li_2S Cathode with High Materials Utilization for All-Solid-State Li/S Batteries Through an Interfacial Redox Mediator. *Adv. Funct. Mater.* **2024**, *34*, 2306939.
107. Shen, K.; Shi, W.; Song, H.; Zheng, C.; Yan, Y.; Hong, X.; Liu, X.; An, Y.; Li, Y.; Ye, F. Solid Catholyte with Regulated Interphase Redox for All-Solid-State Lithium-Sulfur Batteries. *Adv. Mater.* **2025**, *37*, 2417171.
108. Song, H.; Münch, K.; Liu, X.; Shen, K.; Zhang, R.; Weintraut, T.; Yusim, Y.; Jiang, D.; Hong, X.; Meng, J. All-Solid-State Li-S Batteries with Fast Solid–Solid Sulfur Reaction. *Nature* **2025**, *637*, 846–853.
109. Wang, D.; Jhang, L.-J.; Kou, R.; Liao, M.; Zheng, S.; Jiang, H.; Shi, P.; Li, G.-X.; Meng, K.; Wang, D. Realizing High-Capacity All-Solid-State Lithium-Sulfur Batteries Using a Low-Density Inorganic Solid-State Electrolyte. *Nat. Commun.* **2023**, *14*, 1895.
110. Xu, X.; Liu, W.; Kim, Y.; Cho, J. Nanostructured Transition Metal Sulfides for Lithium Ion Batteries: Progress and Challenges. *Nano Today* **2014**, *9*, 604–630.
111. Kim, H.; Choi, H.-N.; Hwang, J.-Y.; Yoon, C. S.; Sun, Y.-K. Tailoring the Interface Between Sulfur and Sulfide Solid Electrolyte for High-Areal-Capacity All-Solid-State Lithium-Sulfur Batteries. *ACS Energy Lett.* **2023**, *8*, 3971–3979.
112. Alzahrani, A. S.; Otaki, M.; Wang, D.; Gao, Y.; Arthur, T. S.; Liu, S.; Wang, D. Confining Sulfur in Porous Carbon by Vapor Deposition to Achieve High-Performance Cathode for All-Solid-State Lithium-Sulfur Batteries. *ACS Energy Lett.* **2021**, *6*, 413–418.
113. Shin, M.; Gewirth, A. A. Incorporating Solvate and Solid Electrolytes for All-Solid-State Li_2S Batteries with High Capacity and Long Cycle Life. *Adv. Energy Mater.* **2019**, *9*, 1900938.
114. Kirchhoff, S.; Fiedler, M.; Dupuy, A.; Härtel, P.; Semmler, M.; Hippauf, F.; Dörfler, S.; Schumm, B.; Abendroth, T.; Althues, H. A Small Electrolyte Drop Enables a Disruptive Semisolid High-Energy Sulfur Battery Cell Design via an Argyrodite-Based Sulfur Cathode in Combination with a Metallic Lithium Anode. *Adv. Energy Mater.* **2024**, *14*, 2402204.
115. Kim, H.; Kim, M. J.; Shin, M. S.; Choi, H. N.; Belharouak, I.; Sun, Y. K. High-Areal-Capacity Sulfur Cathode Enabled by Dual-Phase Electrolyte for Sulfide-Based All-Solid-State Batteries. *Adv. Energy Mater.* **2025**, *15*, 2500867.
116. Wang, C.; Kim, J. T.; Wang, C.; Sun, X. Progress and Prospects of Inorganic Solid-State Electrolyte-Based All-Solid-State Pouch Cells. *Adv. Mater.* **2023**, *35*, 2209074.
117. Hippauf, F.; Schumm, B.; Doerfler, S.; Althues, H.; Fujiki, S.; Shiratsuchi, T.; Tsujimura, T.; Aihara, Y.; Kaskel, S. Overcoming Binder Limitations of Sheet-Type Solid-State Cathodes Using a Solvent-Free Dry-Film Approach. *Energy Storage Mater.* **2019**, *21*, 390–398.
118. Hu, J.-K.; Yuan, H.; Yang, S.-J.; Lu, Y.; Sun, S.; Liu, J.; Liao, Y.-L.; Li, S.; Zhao, C.-Z.; Huang, J.-Q. Dry Electrode Technology for Scalable and Flexible High-Energy Sulfur Cathodes in All-Solid-State Lithium-Sulfur Batteries. *J. Energy Chem.* **2022**, *71*, 612–618.

DOI: 10.31635/ccschem.025.202506213
Citation: *CCS Chem.* **2025**, 7, 3235–3258
Link to VoR: https://doi.org/10.31635/ccschem.025.202506213

119. Fiedler, M.; Cangaz, S.; Hippauf, F.; Dörfler, S.; Abendroth, T.; Althues, H.; Kaskel, S. Mechanistic Insights into the Cycling Behavior of Sulfur Dry-Film Cathodes. *Adv. Sustain. Syst.* **2023**, *7*, 2200439.

120. Lv, Z.; Liu, J.; Li, C.; Peng, J.; Zheng, C.; Zheng, X.; Wu, Y.; Xia, M.; Zhong, H.; Gong, Z.; Yang, Y. High-Areal-Capacity All-Solid-State Li-S Battery Enabled by Dry Process Technology. *eTransportation* **2024**, *19*, 100298.

DOI: 10.31635/ccschem.025.202506213
Citation: *CCS Chem.* **2025**, 7, 3235–3258
Link to VoR: https://doi.org/10.31635/ccschem.025.202506213